A Thin Film Approach to Rapid, Quantitative Measurements of Mixed-Gas Adsorption Equilibrium in Nanoporous Materials

*Jessica C. Moreton,[a] Rajamani Krishna,[b] Jasper M. van Baten,[b] Nicholas Fylstra,[c] Michel Chen,[a] Thomas Carr,[a] Kamalani Fielder,[a] Kristi Chan,[a] George K. H. Shimizu,[c] Steve Yamamoto[a]**

[a] Matrix Sensors, Inc. San Diego, CA, 92121, United States.

[b] University of Amsterdam, Van't Hoff Institute for Molecular Sciences, 1098 XH Amsterdam, The Netherlands

[c] Department of Chemistry, University of Calgary, Calgary, Alberta, Canada

KEYWORDS Adsorption, Desorption, Gases, Mixtures, Carbon Capture, Mixture-adsorption Equilibrium, Metal-organic Frameworks, Nanoporous

Abstract

Nanoporous adsorbent materials are a key part of many industrial processes, including the rapidly-expanding carbon capture industry. Development of advanced sorbents requires an assessment of the sorbent's performance under mixed-gas conditions. Existing measurement techniques tend to be slow, material-intensive, and have limited ability to measure competitive mixed-gas sorption. We have developed a novel technique that measures thin films of sorbents deposited onto sensitive

micro-electromechanical system (MEMS) transducers. This technique is fast, requires very little material, and enables real-time monitoring of binary gas sorption. We report measurements of CO_2/H_2O mixed-gas isotherms at three different temperatures on the carbon capture MOF CALF-20. The measured experimental data on CO_2/H_2O mixture adsorption in CALF-20 demonstrate the severe limitations of the Ideal Adsorbed Solution Theory (IAST) in providing a quantitative estimation of the component loadings. Departures from the IAST are quantified by introduction of activity coefficients and use of the Real Adsorbed Solution Theory (RAST).

Adsorbent materials span a range of important industrial applications including gas separations,[1] gas storage,[2] and carbon capture[3] from both point sources and directly from the atmosphere to mitigate the effects of climate change. The practical implementation of adsorbents into an industrial process often requires a quantitative understanding of the material's adsorption and desorption properties under mixed gas conditions.[4–6] Without this detailed understanding, both the selection of a material and the design of a separation process can become slow and tedious and may rely on optimization through trial-and-error that is often based on flawed extrapolations of simpler separations.

Today there are many commercially available instruments[6] capable of measuring adsorption properties of materials including porosimeters, dynamic vapor sorption (DVS), thermo-gravimetric analysis (TGA), gravimetric or volumetric physisorption, and column breakthrough (CB). While these instruments have standardized the measurement of single-component gas adsorption, their ability to characterize mixed-gas adsorption is often limited. In the absence of experimental data on the mixture adsorption equilibrium, researchers may rely on the use of the Ideal Adsorbed Solution Theory (IAST) of Myers and Prausnitz[7] to quantify and compare mixture

separation performance. The IAST description of mixture adsorption equilibrium relies on a number of basic tenets: (a) homogeneous distribution of guest adsorbates, (b) no preferential locations of any guest species within the pore landscape, and (c) no molecular clustering due to say hydrogen bonding between pairs of adsorbates.[8–14] In a number of publications on CO_2 capture from mixtures containing N_2, CH_4, C_2H_4, C_2H_6, C_3H_8, and H_2O using cation-exchanged zeolites,[8,10,12–19] the IAST has been shown to fail due to non-compliance with one or more of the afore-mentioned tenets.

We report here a new experimental technique for rapid and direct measurements of binary polar/non-polar gas mixtures. This technique measures adsorbent materials in the form of thin films, a form-factor that enables the use of compact micro-electromechanical system (MEMS) measurement devices with very high sensitivity. We use two types of transducers: 1) gravimetric, and 2) electrical capacitance. The gravimetric transducer is a quartz crystal microbalance (QCM), and the electrical capacitance transducer is an interdigitated electrode (IDE) capacitor. The QCM measures the total mass of both species in the binary gas mixture, and the IDE response is dominated by only the polar species.

This thin film technique has several advantages including measurement speed and low material requirements. The measurement speed of equilibrium gas adsorption is often limited by the equilibration time of the material, typically a diffusion-limited process.[6] The equilibration time of even small amounts of bulk powders can be hours or even days for a single data point, especially in the case of separations involving water.[20–22] The thin films in the technique reported here are typically <10 microns thick with equilibration times that are typically tens of minutes to 2 hours, representing a 10x to 20x improvement in measurement speed. Furthermore, the thin films have very low material quantity requirements and can be made with <100 mg of starting powder.

We apply this technique to competitive CO_2 and water sorption in Calgary Framework (CALF)-20,[20] a metal-organic framework (MOF) adsorbent that is used commercially for post-combustion carbon capture. In this case, the QCM measures total sorption of CO_2 and water, while the IDE measures sorption of water only. Through careful calibration and signal processing, we obtain a direct measurement of the amount of CO_2 and water adsorbed into the CALF-20 material (See Figure 1). Using this technique, we report, for the first time, experimental data that illustrates the humidity-dependent nature of thermodynamic non-idealities on CALF-20 adsorption capacity.

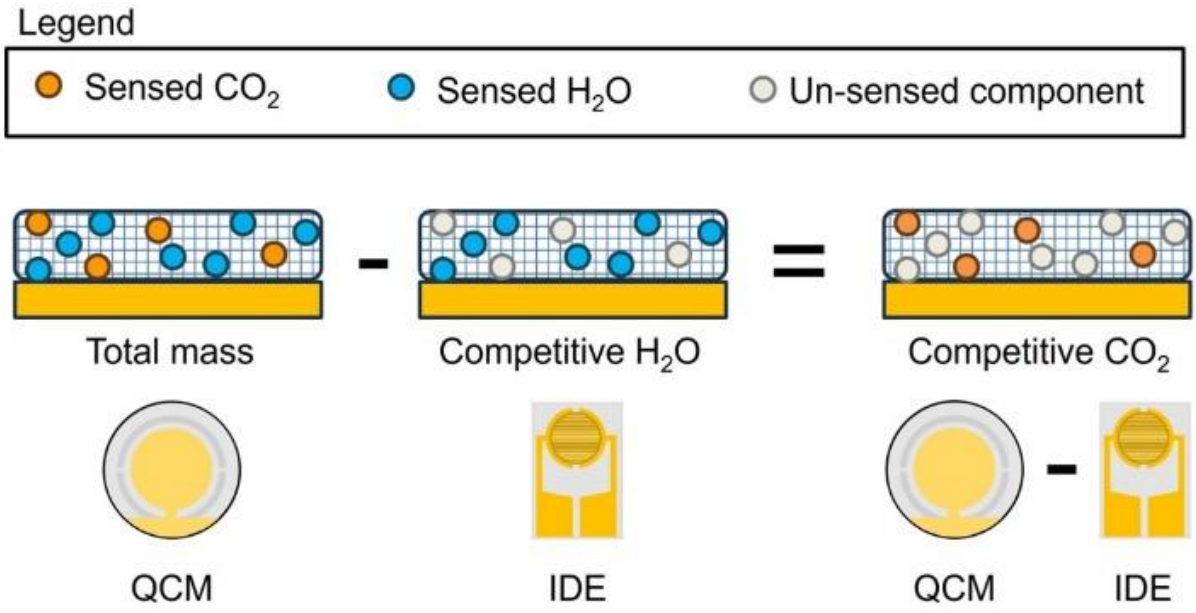

Figure 1. Illustration of how the sorption of polar (e.g. water, blue circles) and non-polar (e.g. CO_2, orange circles) species can be separately measured using the thin film technique reported here. A QCM measures the total mass of all species (e.g. CO_2 and water) adsorbed in the material. An interdigitated electrode (IDE) capacitor measures the dielectric of the material which varies with the amount of adsorbed polar species (e.g., water) and can be converted to mass of water present. Subtracting the two calibrated signals results in the mass of the non-polar species (e.g. CO_2).

The process of obtaining these mixed-gas measurements proceeded as follows:

1) Initial characterization: The MOF was characterized to ensure the integrity of the starting material.
2) Sample preparation: An ink was then formed from MOF powder and a polymer binder. This MOF ink was cast onto the QCM and IDE transducers.
3) Instrument setup: The QCM and IDE samples were mounted in identical flow cells, placed into the measurement system, and a specific test sequence was programmed.
4) Data collection and analysis: The instrument executed the gas test sequence and recorded data from the QCM, IDE, and environmental sensors.
5) Data analysis was performed to generate the reported isotherms and compare to in-house and literature measurements by different techniques.

Further details may be found in the Experimental Section and the supporting information.

The starting powder measurements replicate those reported in the literature.[20] Crystallinity as assessed by PXRD matches the literature-reported data (Figure S1). CO_2 sorption at 273 K was measured by porosimetry and shown to be comparable to that reported in the literature. The 273 K isotherm was measured independently at University of Calgary (Micromeritics ASAP 2460) and at Matrix Sensors (Micromeritics 3Flex). These isotherms agree to within 5%, verifying the quality of the starting material (Figure S2). SEM imaging was conducted at Matrix Sensors and shows that particle sizes are < 7 μm (Figure S3). The thin films, as-cast on the QCM, show MOF particles embedded in polymer uniformly across the surface of the substrates. The particle sizes in the thin films range from submicron to about 7 μm, which is similar to the estimate obtained from SEM imaging of the powder alone (Figures S4, S5). TGA degradation measurements to assess the MOF

content[23,24] of the films are within 10% of the expected MOF content based on initial ink composition (see discussion in supporting information and Figure S6).

Thin film quality was further assessed by a measurement of the quality factor (Q) of the QCM resonator. Generally, a Q>10,000 is needed for high-sensitivity mass measurements; the Q of this sample is approximately 89,000. Details may be found in the SI.

The frequency of the QCM is tracked throughout the duration of the test and is used to determine the total mass of gas adsorbed into the CALF-20 film. The sample is equilibrated at the intended test temperature to establish a baseline. As gases are introduced (Figure 2a), the frequency change of the QCM enables mass calculation by the Sauerbrey equation.[25]

The IDE capacitance (pF) of the CALF-20 film is read out using a bridge circuit. A capacitor measures the dielectric constant of the material between its electrodes. This dielectric constant varies with the presence of polar species. This is the basis of most commercial humidity sensors.[26] As water and CO_2 adsorb into the thin film, the capacitance is only slightly affected by the presence of CO_2 but responds very strongly to water (Figure 2b). The CO_2 capacitance response over the range of CO_2 concentrations used (0-0.5 bar CO_2) is <2% of the relative humidity capacitance response over the range of humidities tested (Figure S7) and we therefore treat it as negligible for the purposes of data analysis, and assign all capacitance response to water. See the supporting information for further discussion.

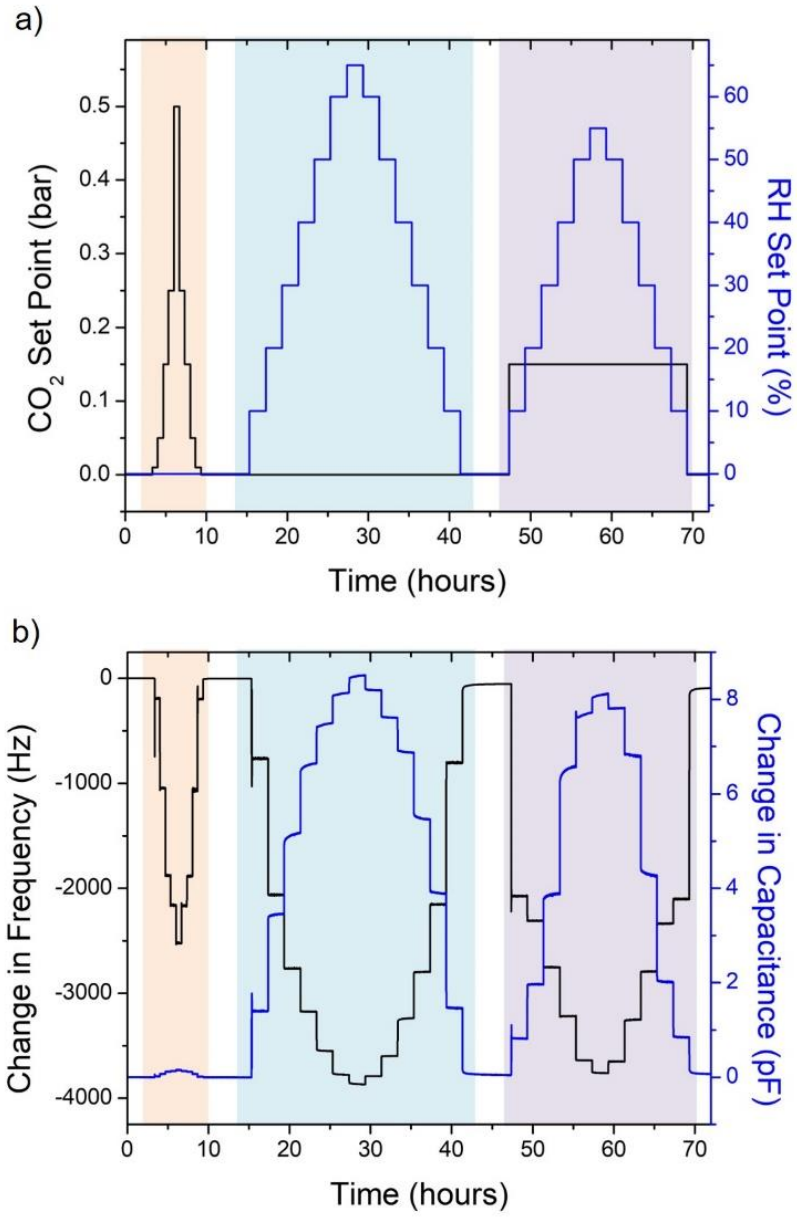

Figure 2. a) A representative test sequence for measurement of CO_2, H_2O, and mixed-gas isotherms showing the CO_2 and RH (relative humidity) set points during the test. This test sequence was run at several different temperatures, including 308 K. b) Representative raw, uncorrected frequency change and capacitance change from the CALF-20 thin films on QCM and IDE sensors, respectively, at a test temperature of 308 K. In both plots, the pink shaded region indicates the CO_2

isotherm; the blue-shaded region indicates the H_2O isotherm; and the purple-shaded region indicates the mixed-gas isotherm at constant 0.15 bar CO_2.

The resonant frequency of a QCM changes in response to mass gain or loss on its surface. Thus, the change in frequency before and after thin film formation, dF_{film}, is proportional to the total mass of the film. During an adsorption test, gas concentrations of interest are introduced in sequential steps. The resulting change in QCM frequency dF_{change} is proportional to the change in total adsorbed species in the material, and the ratio of dF_{change} to dF_{film} produces a weight percent loading in (g adsorbed species)/(g sorbent). In single gas measurements, this value represents the sorption of the single component present (either CO_2 or water); in mixed-gas conditions, this measurement represents the combined mass of CO_2 and H_2O adsorbed. To prevent overshoots and incomplete sample equilibration from affecting our calculations, the last 10 minutes of each pulse are averaged to obtain isotherm points. Based on previous work,[20] we assume that the sorption of our carrier gas (dry air) is negligible in the MOF.

The IDE capacitor was calibrated by measuring a single-component water isotherm and comparing the IDE capacitor reading to the QCM gravimetric response. A curve fit generated from these points enables the conversion from capacitance to water loading in g/g. This calibration was performed at each test temperature. Specifically, the sample was dried for 24h at 353 K, baselined at the test temperature for a minimum of 3 hours, and a single-component water isotherm was measured on both the IDE and QCM to generate a calibration curve. A comparison of the calibration curves shows differences between test temperatures, but two calibrations at the same temperature are reproducible (Figure S8).

Finally, the uptake values are normalized to eliminate the presence of the polymer in the weight fraction, that is, the denominator of the g/g values is adjusted to reflect only the MOF content of

the film. This step likely introduces the most uncertainty to our uptake measurements since the amount of MOF in the composite is not precisely known.

The CO_2 and water single-gas isotherms on CALF-20 thin films were measured using the QCM (frequency/mass) readout and compared to measurements on powder samples conducted on commonly-used static and dynamic sorption instruments including TGA, DVS, and a porosimeter (Micromeritics 3Flex). The thin film CO_2 sorption, normalized for MOF content only, falls between the TGA and 3Flex data. While it is within 10% of the TGA measurement, it is roughly 17% lower than the isotherm reported by the 3Flex, when comparing data points above 0.1 bar CO_2 (Figure 3a). The observation that the thin film QCM measurements are relatively close to both the TGA and porosimetry measurements is verification that our thin film is representative of the powder. However, the lack of agreement between the TGA and porosimetry measurements on the same powder merits further investigation, discussed in the supporting information.

The thin-film water isotherm was compared to powder measurements collected by DVS, TGA, and 3Flex (Figure 3b and Figure S9). While the DVS measurement agrees well with the thin film (within 5-10%), the TGA measurements are roughly 40% lower, while the 3Flex isotherm is roughly 14% higher than the thin film. These variations are also discussed in the supporting information.

Overall, despite the disagreement between various established dynamic and static sorption techniques, we believe our thin film is representative of the starting powder. The polymer component of our thin film has been shown to absorb negligible amounts of water and CO_2 (Figure S10). We do not believe the polymer is blocking MOF pores to a significant extent[27,28] or interacting with the CALF-20 in a suppressive way (see further discussion in the supporting information).

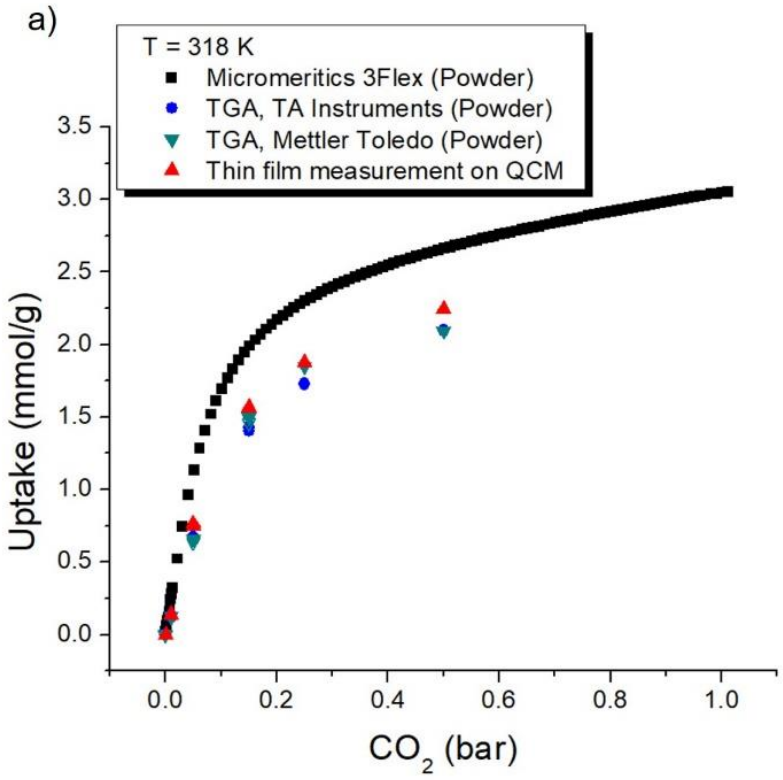
a)
T = 318 K
Micromeritics 3Flex (Powder)
TGA, TA Instruments (Powder)
TGA, Mettler Toledo (Powder)
Thin film measurement on QCM
Uptake (mmol/g)
CO2 (bar)

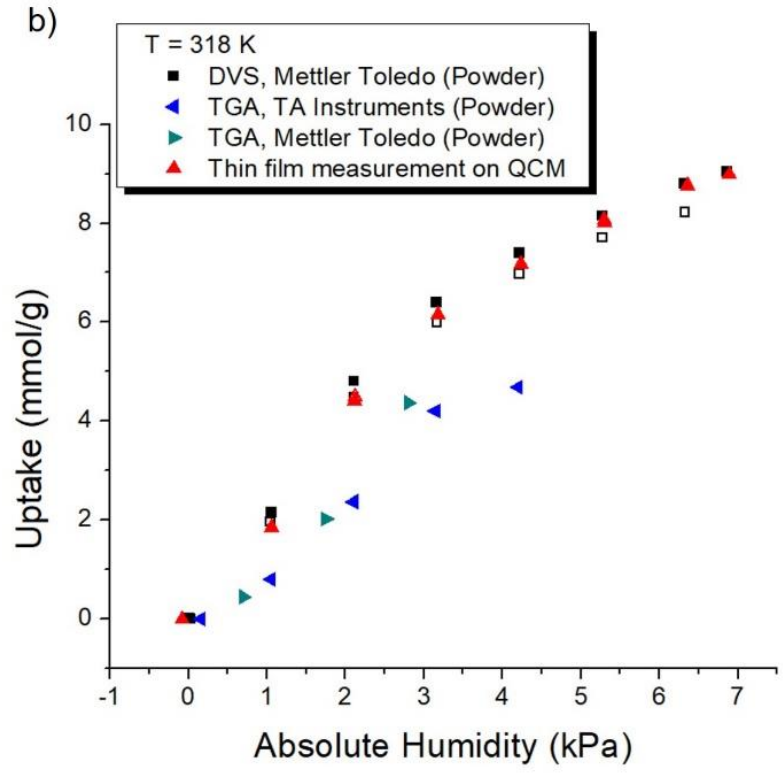
b)
T = 318 K
DVS, Mettler Toledo (Powder)
TGA, TA Instruments (Powder)
TGA, Mettler Toledo (Powder)
Thin film measurement on QCM
Uptake (mmol/g)
Absolute Humidity (kPa)

Figure 3. Thin-film a) CO_2 and b) H_2O single-component isotherms of CALF-20 measured on a QCM, with comparison to powder data obtained by conventional methods: a) TGA and 3Flex and b) DVS and TGA. Filled shapes represent adsorption, and open shapes represent desorption.

Mixed-gas isotherms of CALF-20 thin films are in agreement with results previously published by Shimizu et al (Figure 4a, Figure S11)[20] and others.[22] Several key differences in our isotherm are noted and may be ascribed to different methods of assessment, material composition, and test temperature. Shimizu et al. performed adsorption measurements at 295 K on a structured version of the material composed of 80% CALF-20 and 20% polysulfone. Our sorption measurements are conducted at 298 K on unstructured CALF-20 powder mixed in a non-adsorptive binder. Our calculated isotherms are corrected to remove the wt% of this binder, thereby reporting a normalized MOF-only mass measurement. Due to the ease and speed of data collection, we also obtained mixed-gas desorption isotherms which shows that there is no hysteresis (Figure 4a, Figure S11a).

Analysis of isotherms indicates that unstructured CALF-20 powder has a higher affinity for competitive CO_2 and higher overall loading capacity compared to the structured material reported by Shimizu et al. We furthermore observe the critical inhibitory effect of CO_2 on water adsorption capacity reflected in previous data (Figure S12). The discrepancy in the total uptake of our powder when compared to the Shimizu et al. isotherm is attributed to the polysulfone binder reported in the structured material; CO_2 isotherms reported in Science[20] for the structured CALF-20 show a 25% decrease in adsorption compared to the as-synthesized powder. Comparatively, the difference in adsorption between the structured, literature CALF-20 and our normalized powder isotherm is 17%, which is similar but not identical to the magnitude expected from the structuring of the Shimizu sample. Our isotherm is measured at a slightly higher temperature (298 K vs 295 K) which

is expected to decrease uptake. There are also other effects that are not perfectly controlled that may contribute to the difference, including error in the wt% measurements of our composite ink and MOF dispersion in the bulk versus film composite.

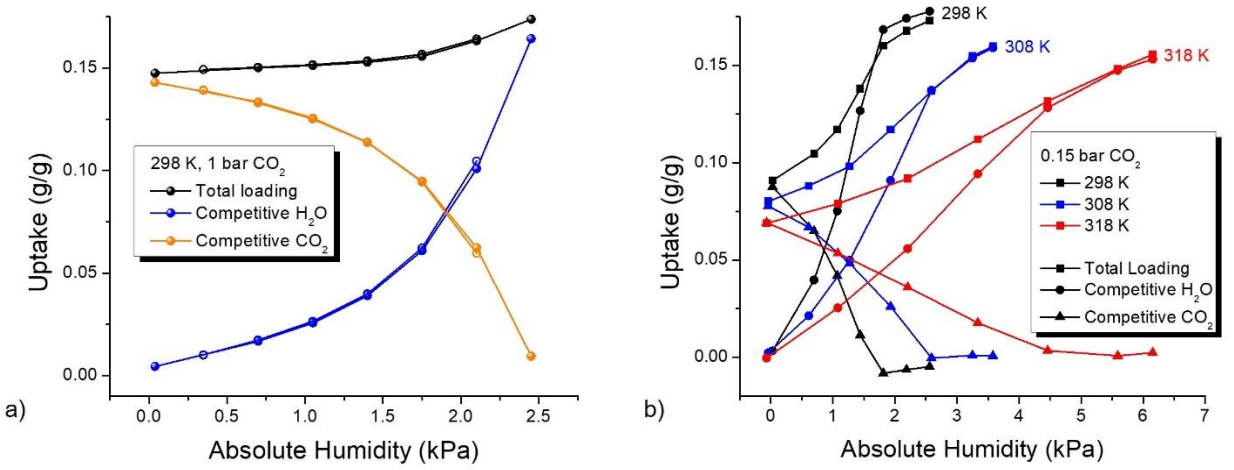

Figure 4. a) Mixed gas isotherms of CO_2/H_2O in a CALF-20 thin film at 100% CO_2 and 298 K showing the competitive adsorption and desorption of CO_2 and H_2O over a range of humidities. At low humidities, CO_2 adsorbs preferentially, while at higher humidities, water dominates. Filled circles represent the adsorption isotherm, and open circles represent the desorption isotherm. b) Mixed-gas isotherms at 0.15 bar CO_2 and temperatures of 298 K, 308 K, and 318 K, plotted using absolute humidity as the x-axis. The data points represent adsorption isotherms only.

For carbon capture applications, it is important to understand how competitive adsorption of water and CO_2 varies with temperature. To explore these temperature effects, we measured mixed gas isotherms on a CALF-20 thin film at three temperatures: 298K, 308K, and 318K. We found that as expected, single-component isotherms of both CO_2 and water decrease with temperature (Figure S13).

Mixed gas water isotherms at a constant CO_2 concentration of 0.15 bar were measured at three temperatures: 298K, 308K, and 318K (Figure 4b and Figure S14). We observe that water uptake

is suppressed at low humidities by CO_2 presence, as was shown in previous work.[20] However, the temperature-dependence of the mixed-gas isotherm exhibits unexpected behavior: Water loading in the MOF decreases significantly with temperature, but CO_2 loading in CALF-20 increases at a given absolute humidity as temperature is increased (Figure 4b). This suggests that raising the temperature of the material and gas stream (assuming a fixed absolute humidity of the gas stream) during operation may extend the range of CO_2 suppression of water loading, further demonstrating the utility of CALF-20 for CO_2 capture in humid conditions. When plotting the same data on a relative humidity scale instead of an absolute pressure scale (Figure S14b), as expected, CO_2 uptake decreases with temperature, as does overall loading. However, water uptake at low relative humidities increases with temperature, further showcasing the competitive effect of CO_2 sorption when water is present: The CO_2 in the MOF diminishes as temperature increases, allowing increased water sorption in this regime. At high relative humidities, the expected trend takes over: Water loading decreases with temperature.

As water loading at 298K reaches saturation, the water loading as measured by the IDE appears to be greater than the total loading reported by the QCM. In the supporting information, we hypothesize two contributing factors for this observation.

The ease of sample deposition and parallelizability of our measurement is demonstrated in a reproducibility study. Two QCM/IDE pairs were cast from the same ink and run simultaneously, demonstrating the parallelizability of our measurement system. The single- and mixed-gas isotherms are nearly identical between the two samples, demonstrating the reproducibility of our method (Figures S15, S16). In the future, we expect to be able to run up to 4 sample pairs simultaneously, which will further increase throughput and offer the possibility of statistical analysis in far less time than conventional methods.

The experimental data on the component loadings of the CO_2(1), and H_2O(2) with varying % relative humidity at three different temperatures 298 K, 308 K, and 318 K measured in this work are indicated by symbols in Figure 5. At each temperature the IAST calculations of mixture adsorption equilibrium, indicated by the dashed line, is unable to quantitatively match the measurements. The failure of the IAST is likely traceable to non-homogeneous distribution of CO_2 and H_2O guests within the channels of CALF-20, along with the formation of hydrogen bonds between pairs of H_2O molecules.[29]

The Real Adsorbed Solution Theory (RAST) model with fitted Margules parameters for describing activity coefficients[9–12,30–32] provide a quantitative match with the experimental measurements; the modeling details are provided in the Supporting Information.

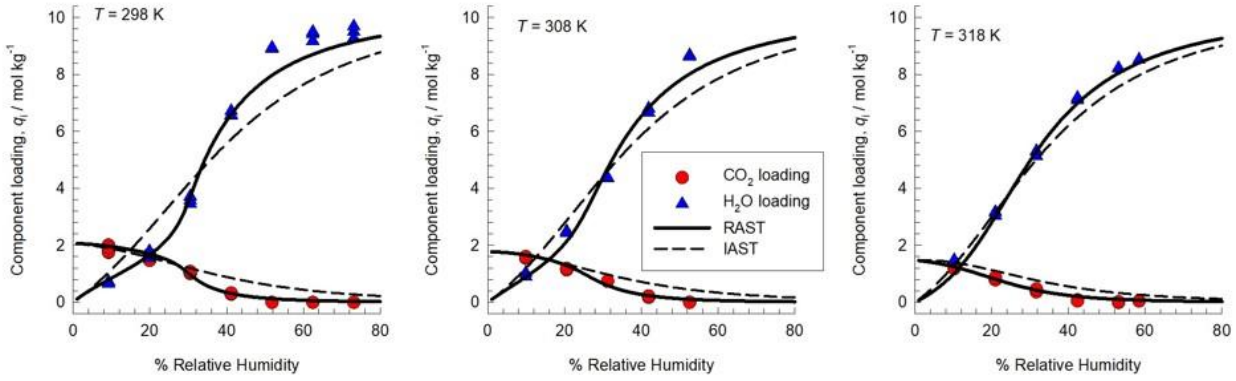

Figure 5. Experimental data obtained in this work (indicated by symbols) on component loadings for CO_2(1)/H_2O(2) mixture adsorption in CALF-20 at 298 K, 308 K, and 318 K. The total pressure in the bulk gas phase is 15 kPa with varying % relative humidity. The dashed lines are the IAST estimations; the continuous solid lines are the estimations using RAST calculations using fitted Margules parameters. The IAST and RAST calculation details, and input data are provided in the Supporting Information accompanying this publication.

We have presented a novel approach to sorbent evaluation that enables rapid measurements of mixed-gas isotherms. The key to our method is the use of a thin-film form factor instead of powders. We validate our thin film approach by demonstrating good correlation of single-component isotherms to standard powder techniques. We also demonstrate that our technique for mixed-gas adsorption reproduces the data from Shimizu et al[20] and others.[21,22] Our test time was approximately 3 days per isotherm, while the mixed-gas isotherm from Shimizu et al would take several weeks to reproduce, albeit on a 16 g column. In other reported techniques, CALF-20 mixed-gas equilibration times were >10 hours[22] and 24 hours[21] per data point, compared to 0.5-2 hours per data point using our thin film method. We additionally measured mixed-gas isotherms at three different temperatures, which allowed us to conduct IAST and RAST modeling of CALF-20. This work underscores the need for the RAST for quantification of CO_2/H_2O mixture adsorption equilibrium by introduction of activity coefficients.

We believe that this experimental technique is expandable to other types of materials, including supported amines and zeolites. Work in progress includes rapid thermal cycling for testing material lifetimes, kinetics and diffusivity. While this method would not necessarily translate directly to the separation performance of a large-scale bed as variables such as heat management and structuring-specific diffusion are not captured, the method provides access to critical data in a facile and timely manner. We anticipate that the thin film approach reported here can accelerate the development of advanced sorbents for DAC and carbon capture industries by accelerating the process of prospective materials evaluation under competitive, real-world relevant conditions.

Experimental Section

Thin film formation, casting, and characterization techniques. CALF-20 powder was combined with an amorphous fluoropolymer binder at a ratio of ~50% MOF, 50% polymer to

create an ink solution that was stirred to homogenize. The solution was cast consecutively onto a quartz crystal microbalance (QCM) and interdigitated electrode (IDE) capacitance device and the resulting thin films were cured under vacuum and characterized. Additional details on ink formulation and thin film casting are provided in the SI.

System details. A schematic of the instrument is shown in Figure S19. The instrument consists of three main components: 1) a gas generator to deliver a gas stream with a controlled flow rate and gas composition, 2) a controlled environmental chamber with gas flow cells containing the mounted QCM and IDE connected in series, and 3) readout and computer control systems. The flow cells have closed-loop temperature control. The gas generator uses infrared CO_2 sensors and capacitive humidity sensors for closed-loop control of the gas mixture and for environmental monitoring inside the flow cell. The capacitive humidity sensor is sensitive to the presence of high levels of CO_2 so a calibration was performed to correct the resulting humidity readings (see SI for details). The readout electronics include a frequency-locked-loop circuit to track the resonant frequency of the QCM and a bridge circuit to monitor the IDE capacitance. A computer controls the entire system, which includes setting gas compositions and recording data from the QCM, IDE, and environmental sensors.

Test sequence. The sample was dried at 353 K under flowing dry air at atmospheric pressure for 24 hours. The sample was then stabilized at the test temperature for several hours until the QCM baseline frequency stabilized. Dry-out and equilibration was performed prior to the start of every isotherm sequence of measurements. Two tests are reported in this work:

1) A reproduction of the mixed-gas adsorption data reported in Science by Shimizu, et al,[20] at 298 K, 1 bar of CO_2, and a range of relative humidities.

2) At each of three temperatures (298 K, 308 K, and 318 K), CO_2 and H_2O single-gas isotherms and a mixed-gas (constant 0.15 bar CO_2) isotherm were measured.

Associated Content

Supporting Information. The following files are available free of charge.

Additional figures, discussion and methods (PDF)

Author Contributions

The manuscript was written through contributions of all authors. All authors have given approval to the final version of the manuscript.

Notes

The authors declare the following competing financial interest(s): J.C.M, M.C., T.C., K.F., K.C., and S.Y. completed this work while employed by Matrix Sensors, Inc., a start-up company working to commercialize mixed-gas testing instrumentation.

7 Acknowledgment

This work was performed in part at the San Diego Nanotechnology Infrastructure (SDNI) of UCSD, a member of the National Nanotechnology Coordinated Infrastructure, which is supported by the National Science Foundation (Grant ECCS-2025752). J. C. M. would like to thank Dr. Julian Hungerford for helpful discussions on adsorption.

8 Abbreviations

IAST, ideal adsorbed solution theory; RAST, real adsorbed solution theory; DVS, dynamic vapor sorption; TGA, thermogravimetric analysis; CB, column breakthrough; QCM, quartz crystal microbalance; IDE, interdigitated electrode; CALF-20, Calgary framework-20; MOF, metal-organic framework; CO_2, carbon dioxide; PXRD, powder X-ray diffraction; SEM, scanning electron microscopy; H_2O, water; MSI, Matrix Sensors, Inc.

9 References

(1) Nandanwar, S. U.; Corbin, D. R.; Shiflett, M. B. A Review of Porous Adsorbents for the Separation of Nitrogen from Natural Gas. *Ind. Eng. Chem. Res.* **2020**, *59* (30), 13355–13369. https://doi.org/10.1021/acs.iecr.0c02730.

(2) Beckner, M.; Dailly, A. Hydrogen and Methane Storage in Adsorbent Materials for Automotive Applications. *Int. J. Energy Res.* **2016**, *40* (1), 91–99. https://doi.org/10.1002/er.3324.

(3) Siegelman, R. L.; Kim, E. J.; Long, J. R. Porous Materials for Carbon Dioxide Separations. *Nat. Mater.* **2021**, *20* (8), 1060–1072. https://doi.org/10.1038/s41563-021-01054-8.

(4) *A Research Agenda for Transforming Separation Science*; National Academies Press, 2019.

(5) Espinal, L.; Poster, D. L.; Wong-Ng, W.; Allen, A. J.; Green, M. L. Measurement, Standards, and Data Needs for CO $_2$ Capture Materials: A Critical Review. *Environ. Sci. Technol.* **2013**, *47* (21), 11960–11975. https://doi.org/10.1021/es402622q.

(6) Shade, D.; Bout, B. W. S.; Sholl, D. S.; Walton, K. S. Opening the Toolbox: 18 Experimental Techniques for Measurement of Mixed Gas Adsorption. *Ind. Eng. Chem. Res.* **2022**, *61* (6), 2367–2391. https://doi.org/10.1021/acs.iecr.1c03756.

(7) Myers, A. L.; Prausnitz, J. M. Thermodynamics of Mixed-Gas Adsorption. *AIChE J.* **1965**, *11* (1), 121–127. https://doi.org/10.1002/aic.690110125.

(8) Krishna, R.; van Baten, J. M.; Baur, R. Highlighting the Origins and Consequences of Thermodynamic Non-Idealities in Mixture Separations Using Zeolites and Metal-Organic Frameworks. *Microporous Mesoporous Mater.* **2018**, *267*, 274–292. https://doi.org/10.1016/j.micromeso.2018.03.013.

(9) Krishna, R.; van Baten, J. M. Fundamental Insights into the Variety of Factors That Influence Water/Alcohol Membrane Permeation Selectivity. *J. Membr. Sci.* **2024**, *698*, 122635. https://doi.org/10.1016/j.memsci.2024.122635.

(10) Krishna, R.; Van Baten, J. M. How Reliable Is the Ideal Adsorbed Solution Theory for the Estimation of Mixture Separation Selectivities in Microporous Crystalline Adsorbents? *ACS Omega* **2021**, *6* (23), 15499–15513. https://doi.org/10.1021/acsomega.1c02136.

(11) Krishna, R.; van Baten, J. M. Water/Alcohol Mixture Adsorption in Hydrophobic Materials: Enhanced Water Ingress Caused by Hydrogen Bonding. *ACS Omega* **2020**, *5* (43), 28393–28402. https://doi.org/10.1021/acsomega.0c04491.

(12) Krishna, R.; van Baten, J. M. Using Molecular Simulations for Elucidation of Thermodynamic Nonidealities in Adsorption of CO2-Containing Mixtures in NaX Zeolite. *ACS Omega* **2020**, *5* (32), 20535–20542. https://doi.org/10.1021/acsomega.0c02730.
(13) Krishna, R.; van Baten, J. M. Elucidation of Selectivity Reversals for Binary Mixture Adsorption in Microporous Adsorbents. *ACS Omega* **2020**, *5* (15), 9031–9040. https://doi.org/10.1021/acsomega.0c01051.
(14) Krishna, R.; van Baten, J. M. Investigating the Non-Idealities in Adsorption of CO2-Bearing Mixtures in Cation-Exchanged Zeolites. *Sep. Purif. Technol.* **2018**, *206*, 208–217. https://doi.org/10.1016/j.seppur.2018.06.009.
(15) Wilkins, N. S.; Rajendran, A. Measurement of Competitive CO2 and N2 Adsorption on Zeolite 13X for Post-Combustion CO2 Capture. *Adsorption* **2019**, *25* (2), 115–133. https://doi.org/10.1007/s10450-018-00004-2.
(16) Hefti, M.; Marx, D.; Joss, L.; Mazzotti, M. Adsorption Equilibrium of Binary Mixtures of Carbon Dioxide and Nitrogen on Zeolites ZSM-5 and 13X. *Microporous Mesoporous Mater.* **2015**, *215*, 215–228. https://doi.org/10.1016/j.micromeso.2015.05.044.
(17) van Zandvoort, I.; Ras, E.-J.; Graaf, R. de; Krishna, R. Using Transient Breakthrough Experiments for Screening of Adsorbents for Separation of C2H4/CO2 Mixtures. *Sep. Purif. Technol.* **2020**, *241*, 116706. https://doi.org/10.1016/j.seppur.2020.116706.
(18) van Zandvoort, I.; van der Waal, J. K.; Ras, E.-J.; de Graaf, R.; Krishna, R. Highlighting Non-Idealities in C2H4/CO2 Mixture Adsorption in 5A Zeolite. *Sep. Purif. Technol.* **2019**, *227*, 115730. https://doi.org/10.1016/j.seppur.2019.115730.
(19) Wang, Y.; LeVan, M. D. Adsorption Equilibrium of Binary Mixtures of Carbon Dioxide and Water Vapor on Zeolites 5A and 13X. *J. Chem. Eng. Data* **2010**, *55* (9), 3189–3195. https://doi.org/10.1021/je100053g.
(20) Lin, J.-B.; Nguyen, T. T. T.; Vaidhyanathan, R.; Burner, J.; Taylor, J. M.; Durekova, H.; Akhtar, F.; Mah, R. K.; Ghaffari-Nik, O.; Marx, S.; Fylstra, N.; Iremonger, S. S.; Dawson, K. W.; Sarkar, P.; Hovington, P.; Rajendran, A.; Woo, T. K.; Shimizu, G. K. H. A Scalable Metal-Organic Framework as a Durable Physisorbent for Carbon Dioxide Capture. *Science* **2021**, *374* (6574), 1464–1469. https://doi.org/10.1126/science.abi7281.
(21) Hastings, J.; Lassitter, T.; Fylstra, N.; Shimizu, G. K. H.; Glover, T. G. Steam Isotherms, CO2/H2O Mixed-Gas Isotherms, and Single-Component CO2 and H2O Diffusion Rates in CALF-20. *Ind. Eng. Chem. Res.* **2024**. https://doi.org/10.1021/acs.iecr.4c00373.
(22) Wang, X.; Alzayer, M.; Shih, A. J.; Bose, S.; Xie, H.; Vornholt, S. M.; Malliakas, C. D.; Alhashem, H.; Joodaki, F.; Marzouk, S.; Xiong, G.; Del Campo, M.; Le Magueres, P.; Formalik, F.; Sengupta, D.; Idrees, K. B.; Ma, K.; Chen, Y.; Kirlikovali, K. O.; Islamoglu, T.; Chapman, K. W.; Snurr, R. Q.; Farha, O. K. Tailoring Hydrophobicity and Pore Environment in Physisorbents for Improved Carbon Dioxide Capture under High Humidity. *J. Am. Chem. Soc.* **2024**, *146* (6), 3943–3954. https://doi.org/10.1021/jacs.3c11671.
(23) Satheeshkumar, C.; Yu, H. J.; Park, H.; Kim, M.; Lee, J. S.; Seo, M. Thiol–Ene Photopolymerization of Vinyl-Functionalized Metal–Organic Frameworks towards Mixed-Matrix Membranes. *J. Mater. Chem. A* **2018**, *6* (44), 21961–21968. https://doi.org/10.1039/C8TA03803A.
(24) Mondal, P.; Cohen, S. M. Self-Healing Mixed Matrix Membranes Containing Metal–Organic Frameworks. *Chem. Sci.* **2022**, *13* (41), 12127–12135. https://doi.org/10.1039/d2sc04345a.
(25) Sauerbrey, G. Verwendung von Schwingquarzen Zur Wägung Dünner Schichten Und Zur Mikrowägung. *Z. Für Phys.* **1959**, *155* (2), 206–222. https://doi.org/10.1007/BF01337937.

(26) Arman Kuzubasoglu, B. Recent Studies on the Humidity Sensor: A Mini Review. *ACS Appl. Electron. Mater.* **2022**, *4* (10), 4797–4807. https://doi.org/10.1021/acsaelm.2c00721.
(27) Baumann, A. E.; Beaucage, P. A.; Vallery, R.; Gidley, D.; Nieuwendaal, R. C.; Snyder, C. R.; Ilavsky, J.; Chen, F.; Stafford, C. M.; Soles, C. L. Assessing Composite Structure in Metal–Organic Framework-Polymer Mixed-Matrix Membranes. *Chem. Mater.* **2024**, *36* (6), 3022–3033. https://doi.org/10.1021/acs.chemmater.4c00283.
(28) Duan, P.; Moreton, J. C.; Tavares, S. R.; Semino, R.; Maurin, G.; Cohen, S. M.; Schmidt-Rohr, K. Polymer Infiltration into Metal–Organic Frameworks in Mixed-Matrix Membranes Detected in Situ by NMR. *J. Am. Chem. Soc.* **2019**, *141* (18), 7589–7595. https://doi.org/10.1021/jacs.9b02789.
(29) Krishna, R.; van Baten, J. M. Elucidating the Failure of the Ideal Adsorbed Solution Theory for CO2/H2O Mixture Adsorption in CALF-20. *Sep. Purif. Technol.* **2025**, *352*, 128269. https://doi.org/10.1016/j.seppur.2024.128269.
(30) Talu, O.; Myers, A. L. Rigorous Thermodynamic Treatment of Gas Adsorption. *AIChE J.* **1988**, *34* (11), 1887–1893. https://doi.org/10.1002/aic.690341114.
(31) Talu, O.; Zwiebel, I. Multicomponent Adsorption Equilibria of Nonideal Mixtures. *AIChE J.* **1986**, *32* (8), 1263–1276. https://doi.org/10.1002/aic.690320805.
(32) Siperstein, F. R.; Myers, A. L. Mixed-Gas Adsorption. *AIChE J.* **2001**, *47* (5), 1141–1159. https://doi.org/10.1002/aic.690470520.

Supporting Information

A Thin Film Approach to Rapid, Quantitative Measurements of Mixed-Gas Adsorption Equilibrium in Nanoporous Materials

*Jessica C. Moreton,[a] Rajamani Krishna,[b] Jasper M. van Baten,[b] Nicholas Fylstra,[c] Michel Chen,[a] Thomas Carr,[a] Kamalani Fielder,[a] Kristi Chan,[a] George K. H. Shimizu,[c] Steve Yamamoto[a]**

[a] Matrix Sensors, Inc. San Diego, CA, 92121, United States

[b] Van't Hoff Institute for Molecular Sciences, University of Amsterdam, 1098 XH Amsterdam, The Netherlands

[c] Department of Chemistry, University of Calgary, Calgary, Alberta, Canada

Contents

1 Experimental Details

1.1 Thin Film Formation and Characterization Procedures

General. CALF-20 was prepared and provided by the Shimizu group at the University of Calgary using a previously reported synthesis method[1] and used as received. All other solvents and starting materials were purchased from chemical suppliers and used without further purification (Sigma Aldrich, Chemours).

MOF/Polymer Ink Preparation. A 6% solution of Teflon AF-1601 in FC-40 (0.166 g polymer) was added to a 10mL vial containing CALF-20 powder (0.149g) to yield an ink targeting 50 wt% MOF. The solution was stirred on a plate (500 rpm, room temperature) to homogenize and was visibly uniform after 4 days. Casting was performed after 28 days of continuous stirring.

Thin Film Casting Details. The surface of a bare QCM and IDE was prepared for deposition via successive solvent rinses of acetone, MeOH, and deionized water (5mL each) and oxidation under a UVO High Intensity Grid Lamp (Jelight, 15 minutes). Immediately before casting, the ink was sonicated for 15 minutes at room temperature and vortexed to ensure uniform suspension. An aliquot of ink was then deposited onto the prepared QCM. The process was immediately repeated with another aliquot of ink to create a second layer. The complete composite was cured at 165°C for 15 minutes. The same procedure was then used to deposit the same ink upon an IDE capacitor. The QCM and IDE were then transferred to a vacuum oven and heated at 105°C for 12h under vacuum.

PXRD. Powder X-ray diffraction (PXRD) spectra was collected on the starting powder at room temperature on a Rigaku MiniFlex 600 with a Cu Kβ filter (Ni/Cu) running at 20kV, 2mA for Cu Kα (λ = 1.5418 Å), with a scan speed of 10°/min, a step size of 0.01° 2θ, and a range of 3 - 50 °2θ. Sample

holders used were zero-background Si well-type plates (depth = 0.2 mm). Computed spectra of CALF-20 (alpha and beta variations) were obtained from literature.[2]

SEM (Zeiss). SEM images of the CALF-20 composite film were taken using a Zeiss Sigma 500 SEM (Carl Zeiss AG).

SEM (Phenom). SEM images of the CALF-20 starting powder were taken using a Phenom XL Desktop SEM (Phenom World).

CO_2 Sorption Analysis. Approximately 80 mg of starting powder was placed in a tared sample tube with filler rod and degassed at 60°C for 2 hours followed by 100°C for 12 hours on a Micromeritics Smart VacPrep. Post-degas, the sample tube was weighed and transferred to a Micromeritics 3Flex Analyzer, where it was degassed for an additional 4 hours at 80°C. CO_2 sorption isotherm data was then collected using a volumetric technique. Sample temperature was controlled by a calibrated Micromeritics IsoController unit filled with a 10% propylene glycol/water solution. Isotherms were run at both 273 K and 298 K.

TGA- Degradation. Thermogravimetric degradation analysis on the starting powder, the polymer binder, and the film was recorded on a TA Instruments Thermogravimetric Analyzer Q500 under a 60 mL/min N_2 stream using an alumina pan at a heating rate of 10°C/min until a 2 h 100°C hold and 5°C/min thereafter up to 800°C.

TGA- Isotherms. Thermogravimetric uptake analysis on the starting powder was recorded on a TA Instruments Thermogravimetric Analyzer Q500 with attached gas generator (same design as in the system described in the manuscript). The flow rate was 60 ml/min and the balance gas used was dry air. The sample was heated to 120 °C until stabilized before holding the temperature at 45°C for the isotherm steps.

DVS. Dynamic vapor sorption measurements for water isotherms on starting powder were taken by a Mettler Toledo Sorption Test System SPSx-1u High Load in aluminum pans using zero air. The samples were held at 60°C under dry air until stabilized before holding the temperature at 45°C for the isotherm steps.

Measurement of Q. QCMs are assessed for test viability after thin-film deposition via Q factor. Q is a dimensionless parameter by which we characterize the quality of our resonant frequency measurement; high oscillator sensitivity is crucial in obtaining precise calculations of the sorption of a gas in our thin film. To measure Q, the admittance of the sample was measured versus frequency. The phase of that admittance was fitted, and the Q was derived from the slope of the fit (f_0 = resonant frequency, φ = phase):

$$Q = \frac{f_0}{2} \times \frac{d\varphi}{df}$$

1.2 Testing Details

Mounting Details. The QCM and IDE samples were mounted in identical environmentally controlled gas flow cells onto ceramic posts within the flow cells using non-conductive epoxy and cured for 15 minutes at 110°C. Gold wires were bonded to the samples using silver conductive epoxy and cured for 30 minutes at 110°C. The mounting provides electrical contact to the devices as well as mechanical strain relief for the QCM.

RH Sensor Correction for CO_2 Presence. A known humidity was delivered to the RH sensor and recorded. CO_2 was then introduced to the humid air stream at a series of known partial pressures from 0.01 to 0.5 bar while keeping the total pressure and flow rate the same. As the CO_2 was introduced, the RH sensor value was recorded. This procedure was performed at a number of humidities, and the actual vs. recorded RH values in the presence of specific CO_2 amounts were fit to a line and used to correct the RH data from tests at that constant CO_2 value.

2 Additional Experimental Results

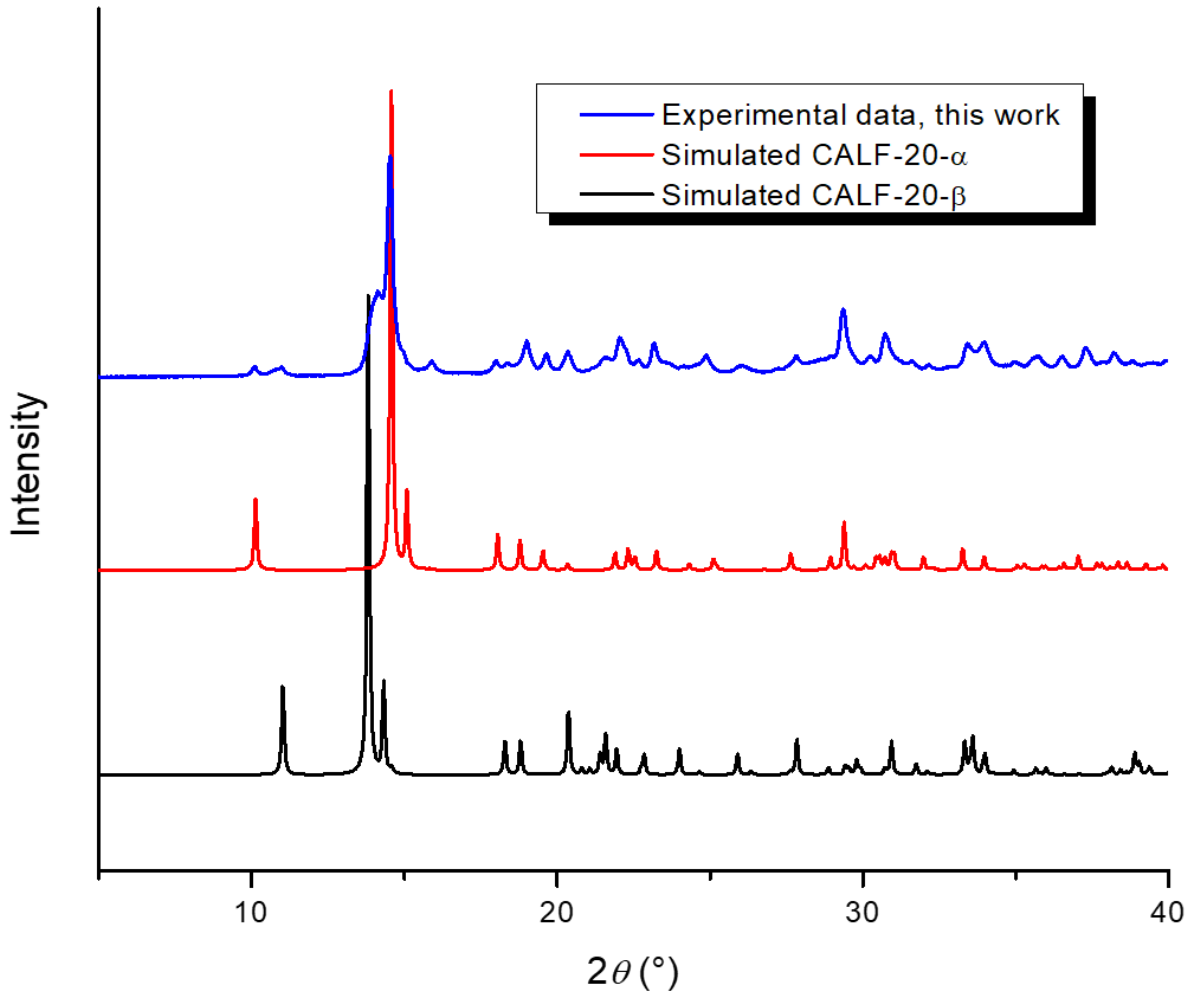

Figure S 1. Powder X-ray diffraction of this CALF-20 sample compared to literature results. CALF-20 is a flexible material with two different powder patterns. Our powder pattern appears to contain peaks from both.

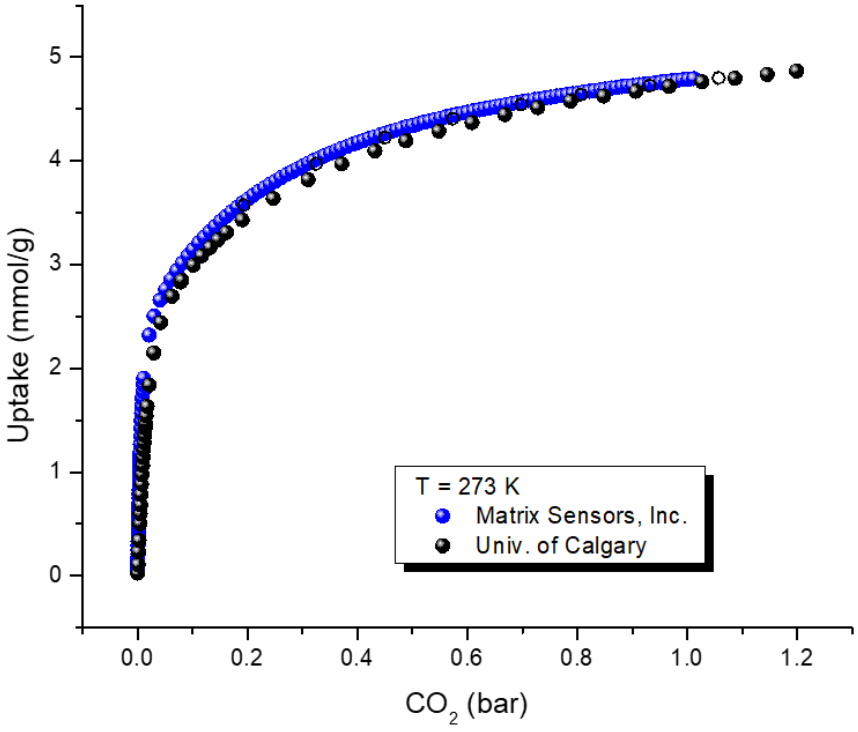

Figure S 2. Physisorption isotherms of the as-received powder, measured at both University of Calgary and Matrix Sensors, Inc. Adsorption points are indicated with filled circles, and desorption points are indicated with open circles. The isotherms are within 5% of each other, indicating good agreement.

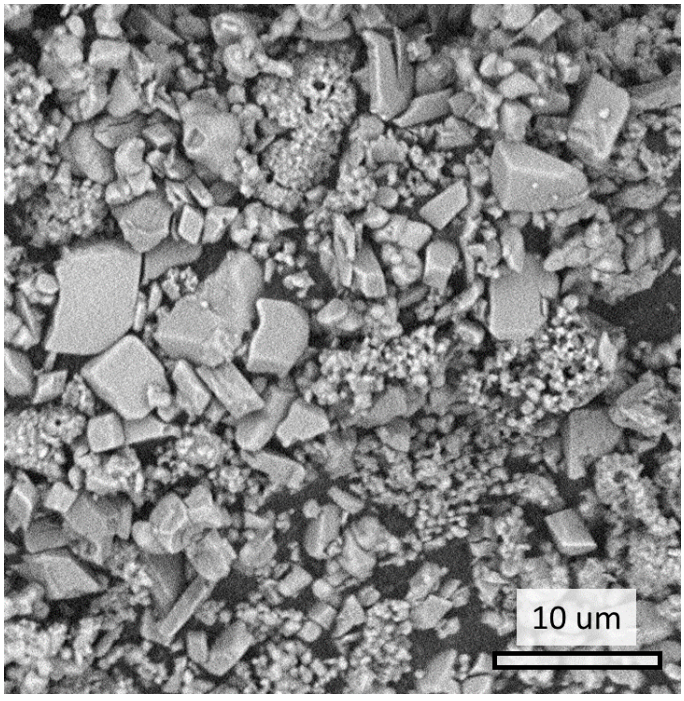

Figure S 3. SEM image of CALF-20 powder at 4500X. Particle sizes range from submicron to ~7 μm.

a)

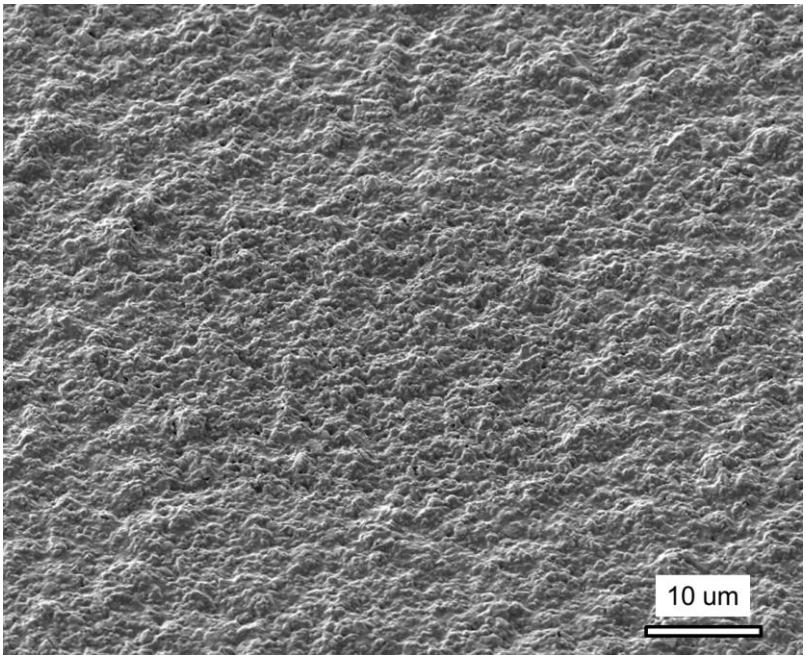

b)

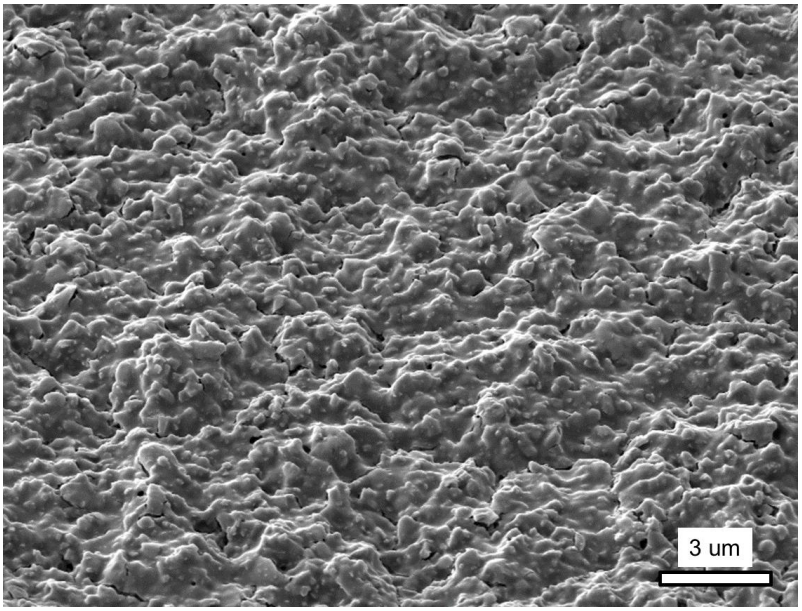

Figure S 4. Top-down SEM images of thin composite films mounted at 45° at two different magnifications. Particles appear reasonably uniformly distributed in a polymer matrix.

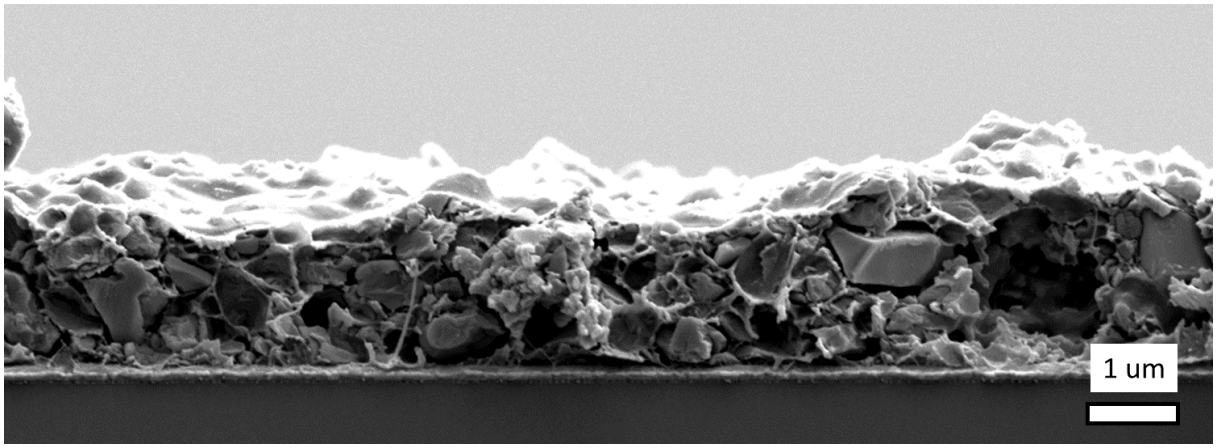

Figure S 5. Cross sectional image of a thin composite film. The film is roughly 2 microns thick.

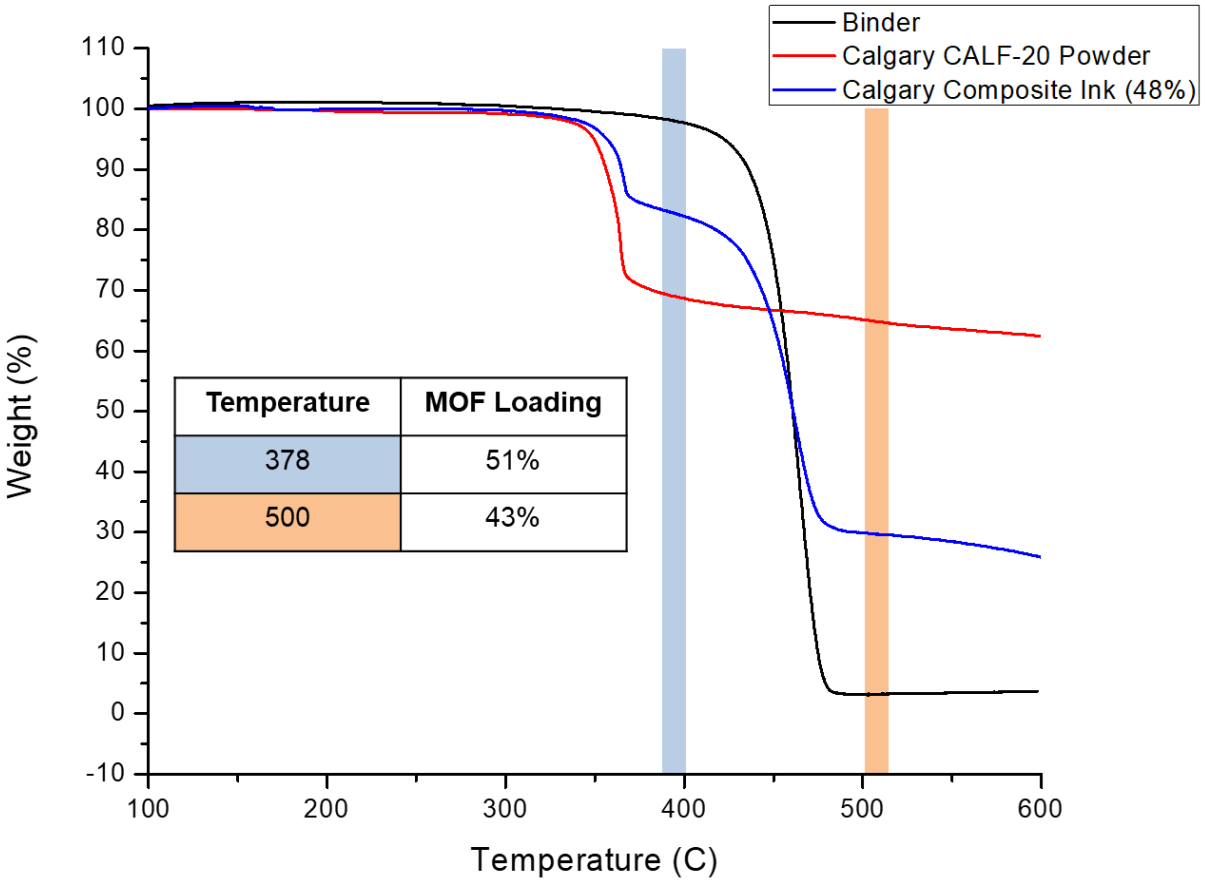

Figure S 6. TGA analysis of composite ink in comparison with Calgary CALF-20 and binder. The highlighted regions are each used to calculate the material loading in the composite ink (see inset table and discussion later in the SI).

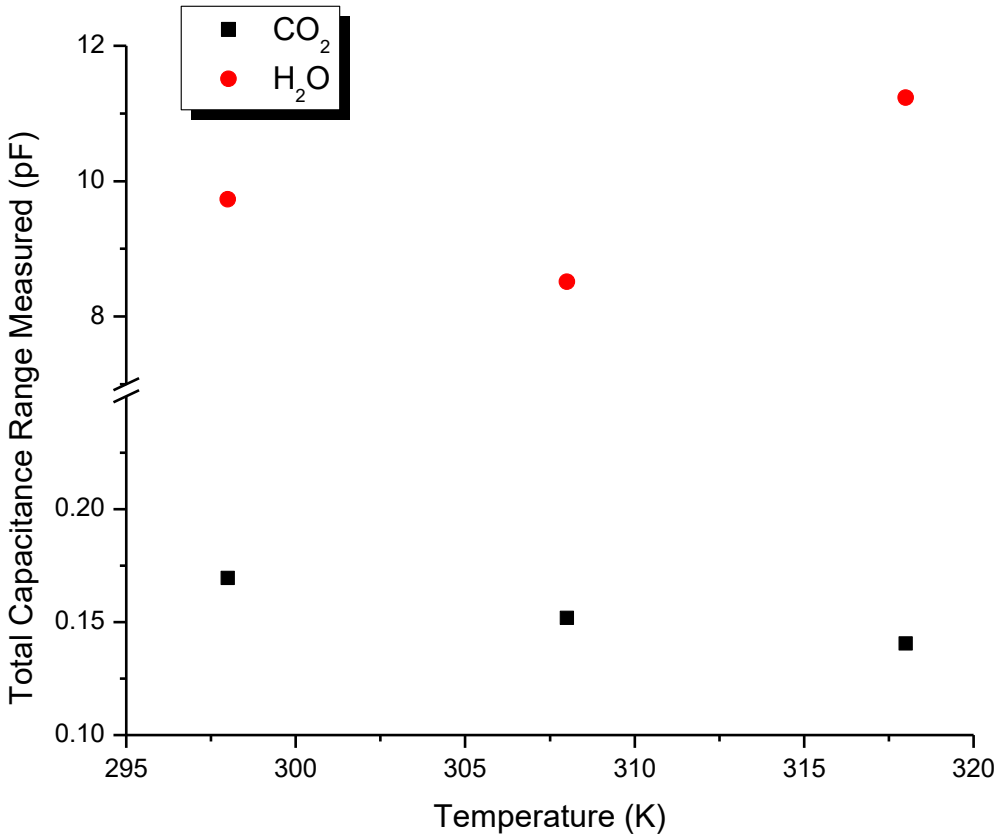

Figure S 7. The total range of CO_2 and water capacitances recorded at each of the three test temperatures is plotted here. The capacitance range for CO_2 represents 0-0.5 bar of CO_2. The capacitance range for water represents 0-85% RH at 298 K, and 0-65% RH for 308 K and 318 K. The magnitude of the CO_2 change over the range tested is < 2% of the H_2O change, which we treat as negligible.

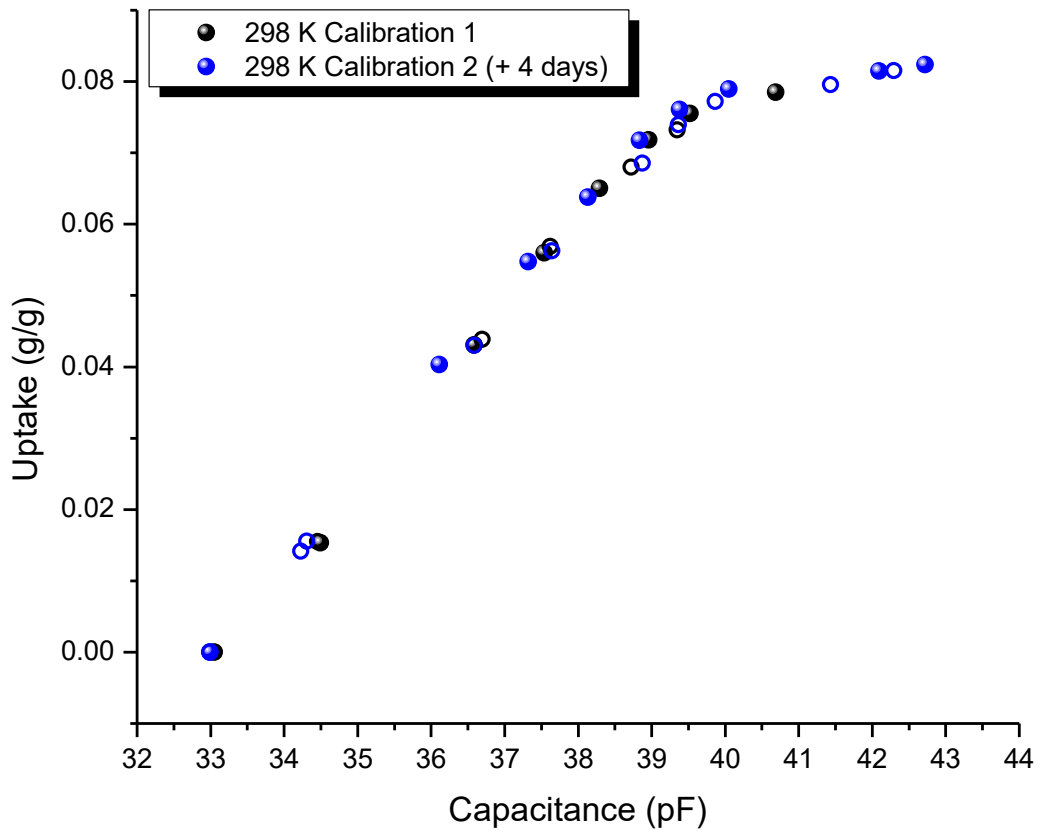

Figure S 8. Comparison between two humidity calibration plots taken at the same temperature on different days, showing slight differences but good agreement. Filled circles indicate adsorption points, and open circles indicate desorption points.

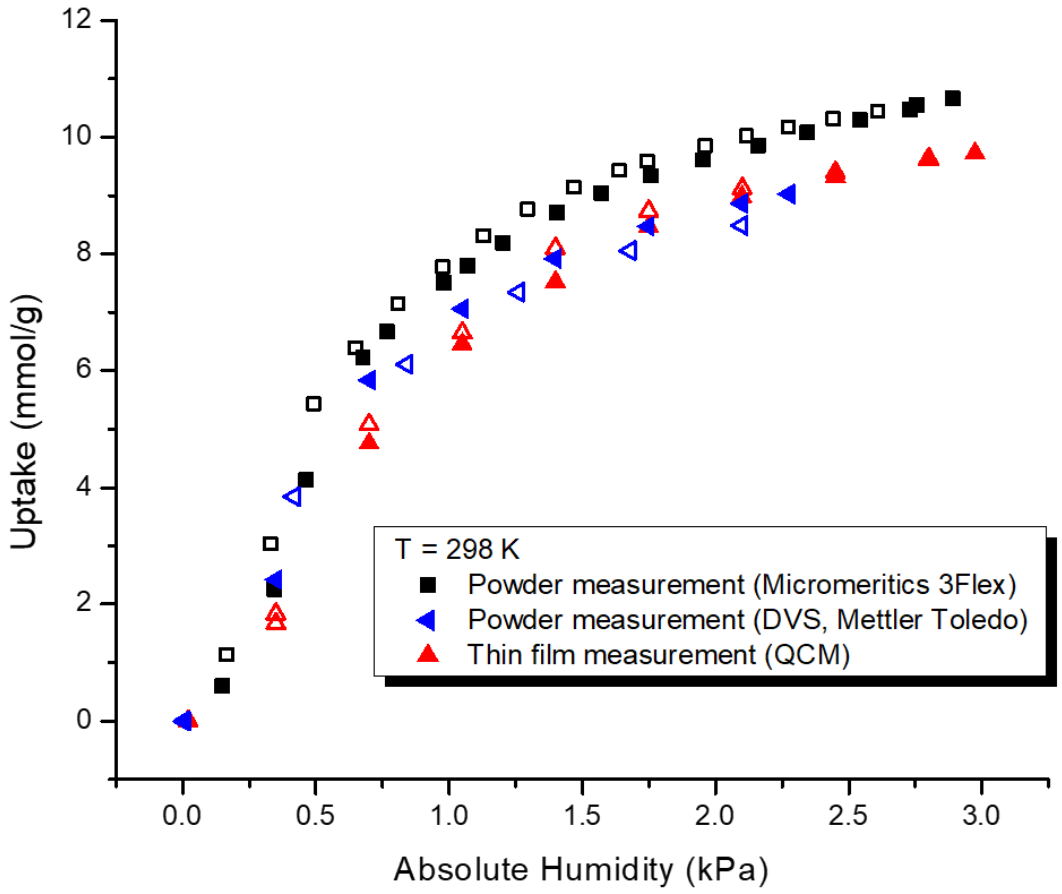

Figure S 9. Powder and thin film measurements at 298 K compared. The thin film QCM measurement is very similar to the measurement of powder on DVS (dynamic vapor sorption), and both are somewhat lower than the static sorption isotherm obtained from a Micromeritics 3Flex.

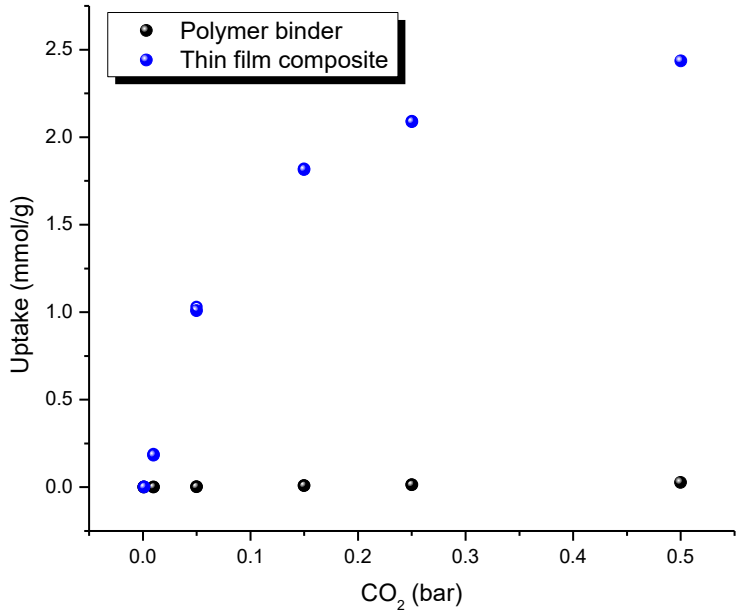

a)

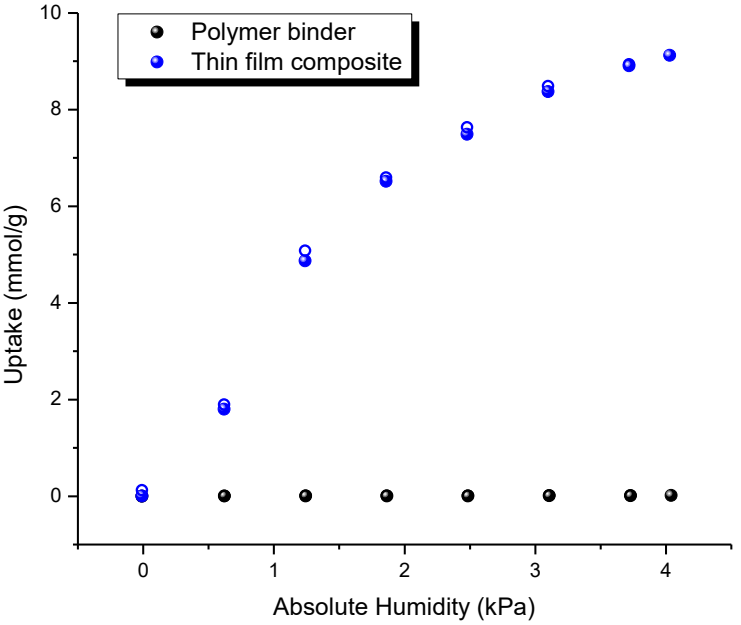

b)

Figure S 10. Comparison of loading in the polymer binder vs. in the composite at 308 K of a) CO_2 and b) H_2O. Filled circles indicate adsorption points and open circles indicate desorption points. The polymer binder takes up essentially zero CO_2 and H_2O in comparison with the composite.

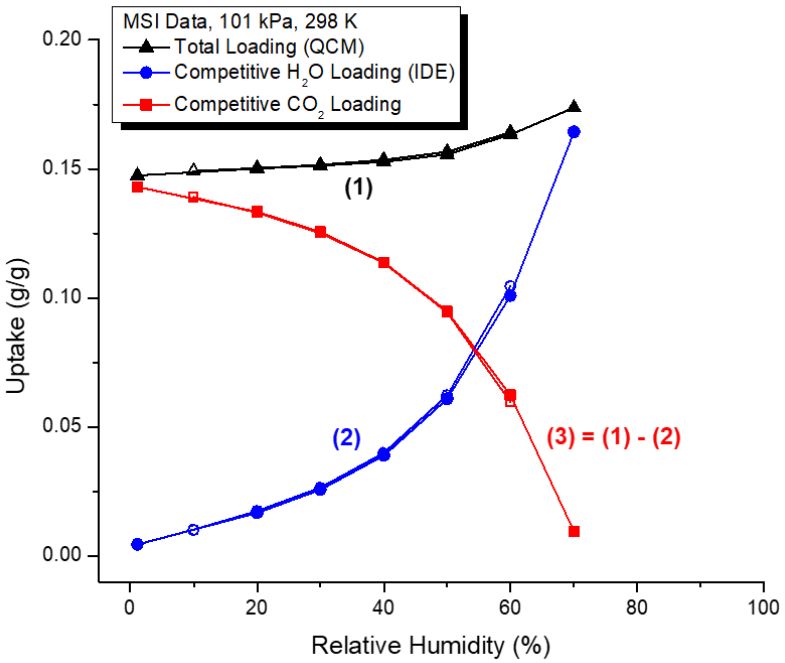

a)

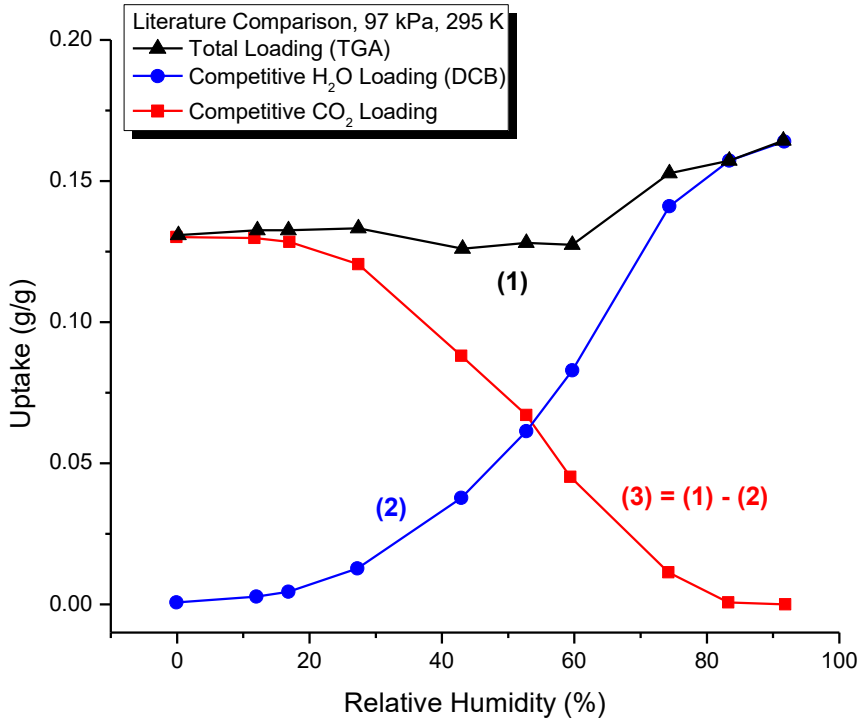

b)

Figure S 11. Mixed-gas sorption of CALF-20 in a CO_2 atmosphere and varying % RH is shown plotted on a relative humidity scale for a) thin films normalized to MOF only at 298 K in this work (1 bar CO_2), and b) structured powder with 20% non-adsorbing binder at 295 K using TGA and column breakthrough (97 kPa CO_2), from Lin, J.-B., et al. A Scalable Metal-Organic Framework as a Durable Physisorbent for

Carbon Dioxide Capture. *Science* **2021**, *374* (6574), 1464–1469. https://doi.org/10.1126/science.abi7281. Reprinted with permission from AAAS.

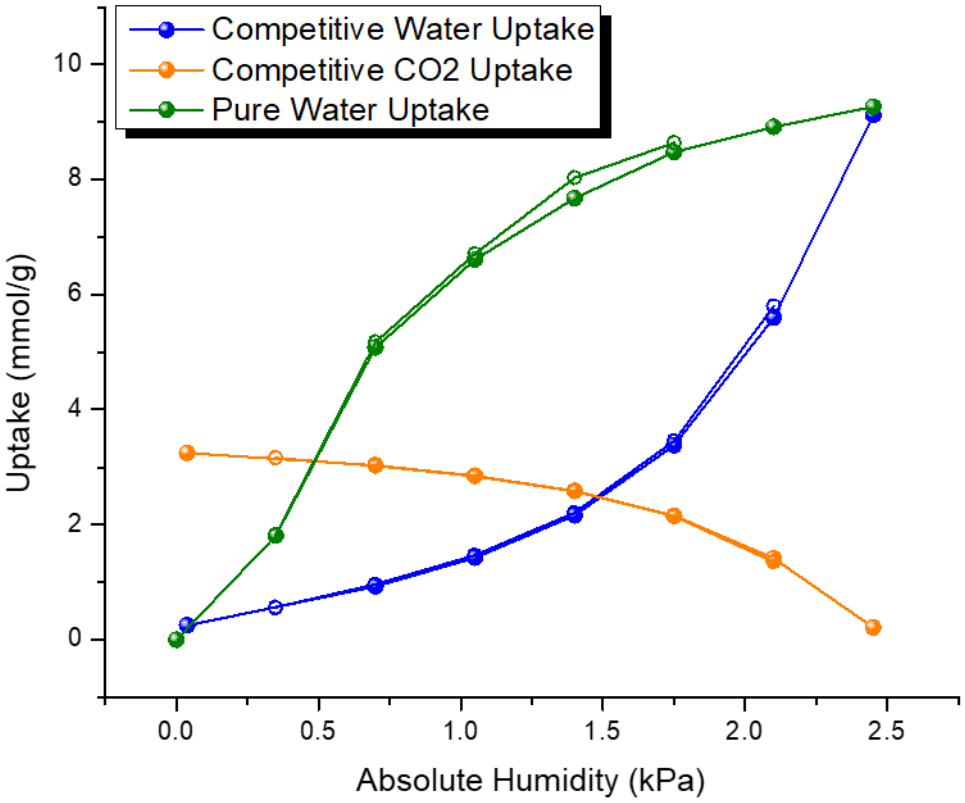

Figure S 12. Mixed-gas sorption of CO_2 and water at 298 K and 1 bar of CO_2, compared to water-only sorption at the same temperature. The comparison of the green and blue traces show that CO_2 presence outcompetes water up to ~1.5 kPa water, and suppresses competitive water uptake compared to water-only uptake up to 2.5 kPa. Filled circles indicate adsorption points and open circles indicate desorption points.

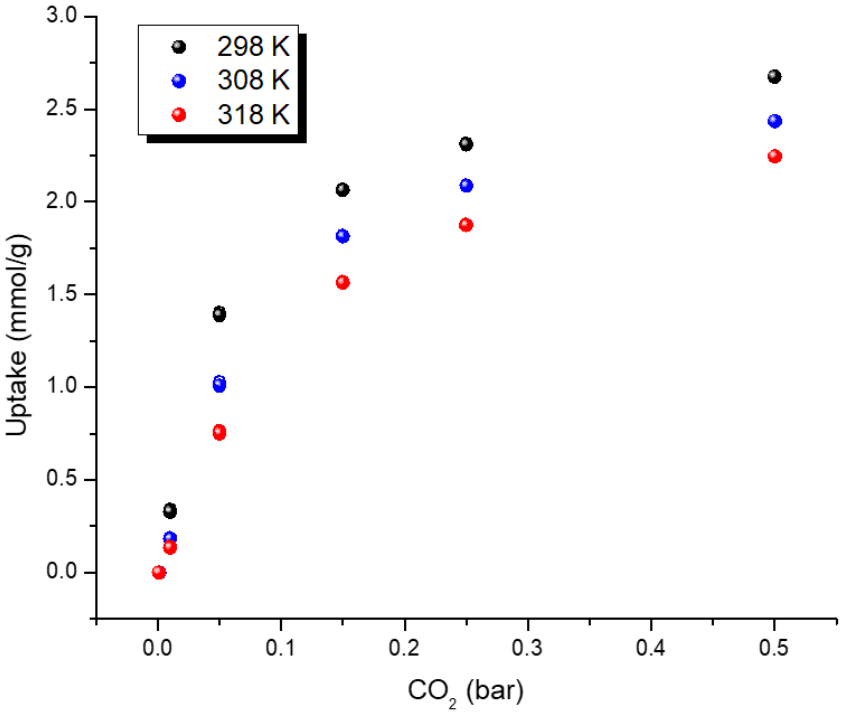

a)

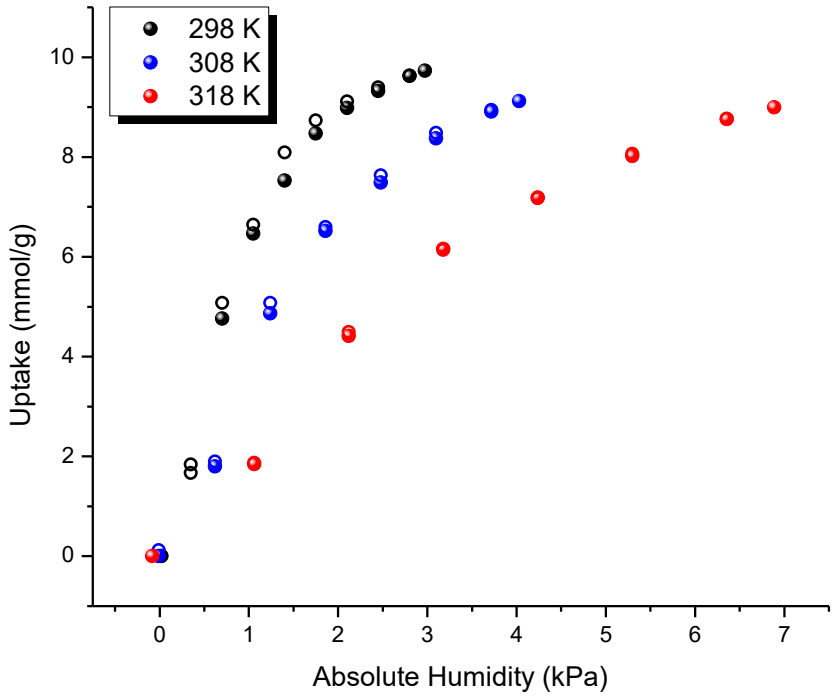

b)

Figure S 13. Single-component isotherms of a) CO_2 and b) H_2O of a CALF-20 thin film on a QCM at three temperatures showing decreasing sorption as temperature increases. Filled circles represent adsorption, and open circles represent desorption isotherms.

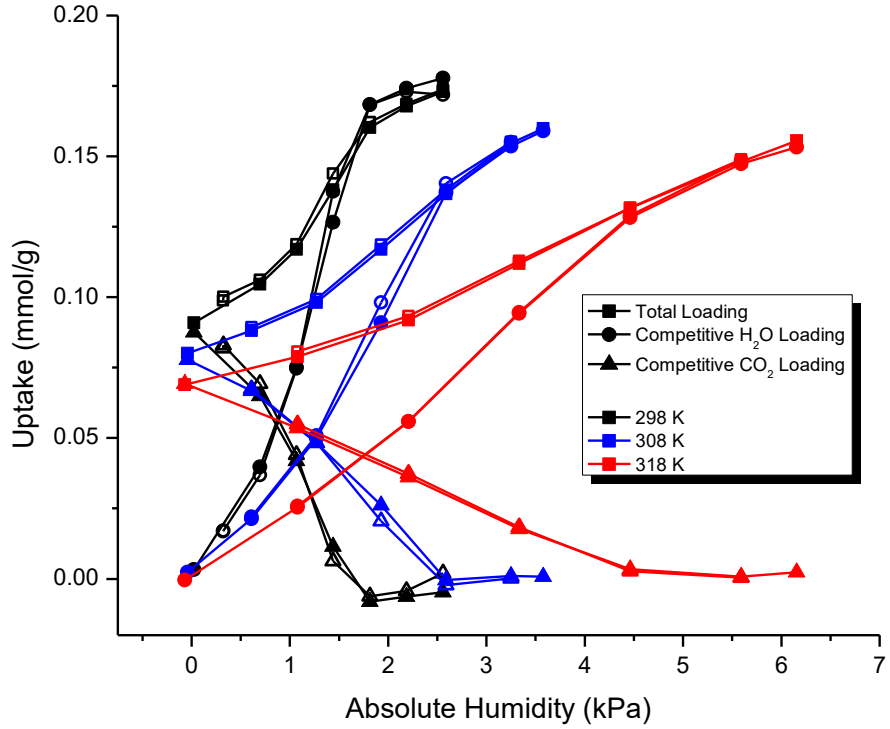

a)

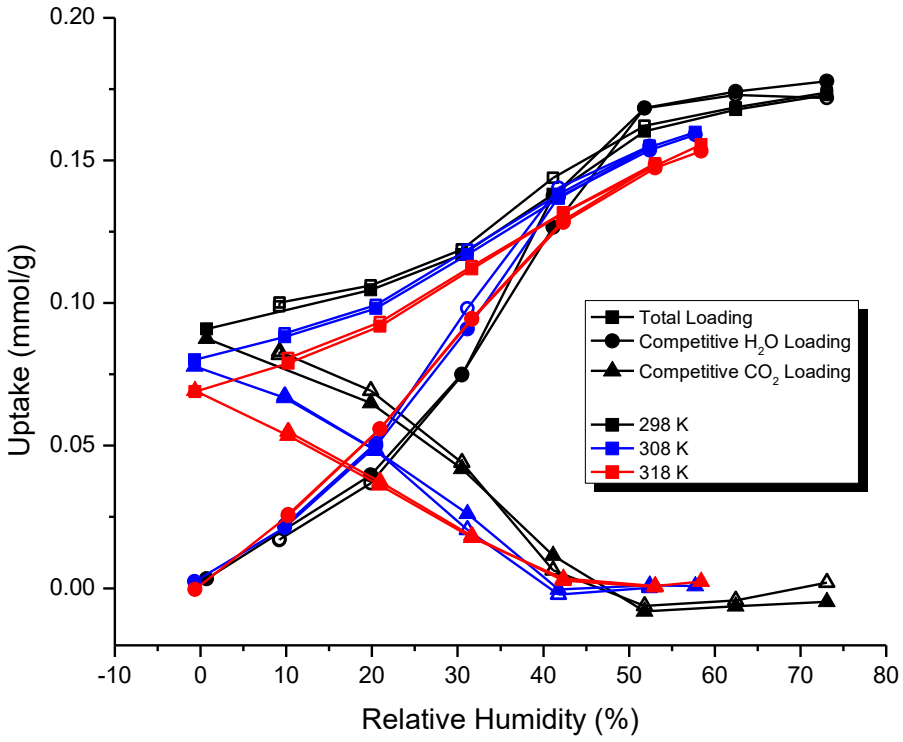

b)

Figure S 14. Temperature series mixed-gas isotherms at 0.15 bar CO_2 at temperatures of 298 K, 308 K, and 318 K, plotted using a) absolute humidity and b) relative humidity as the x-axis. The filled symbols represent the adsorption isotherms, and the open symbols represent the desorption isotherms.

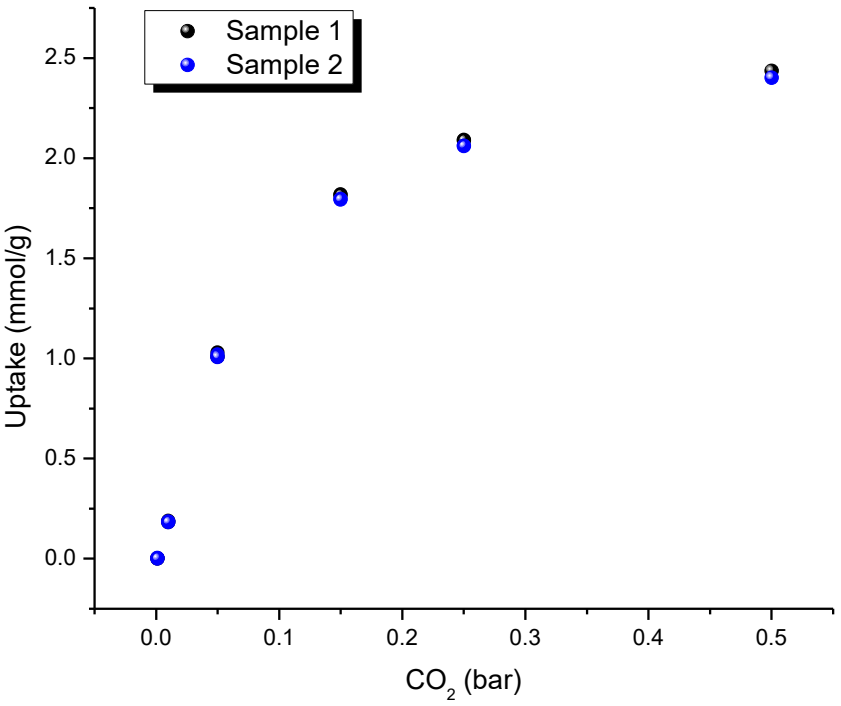

a)

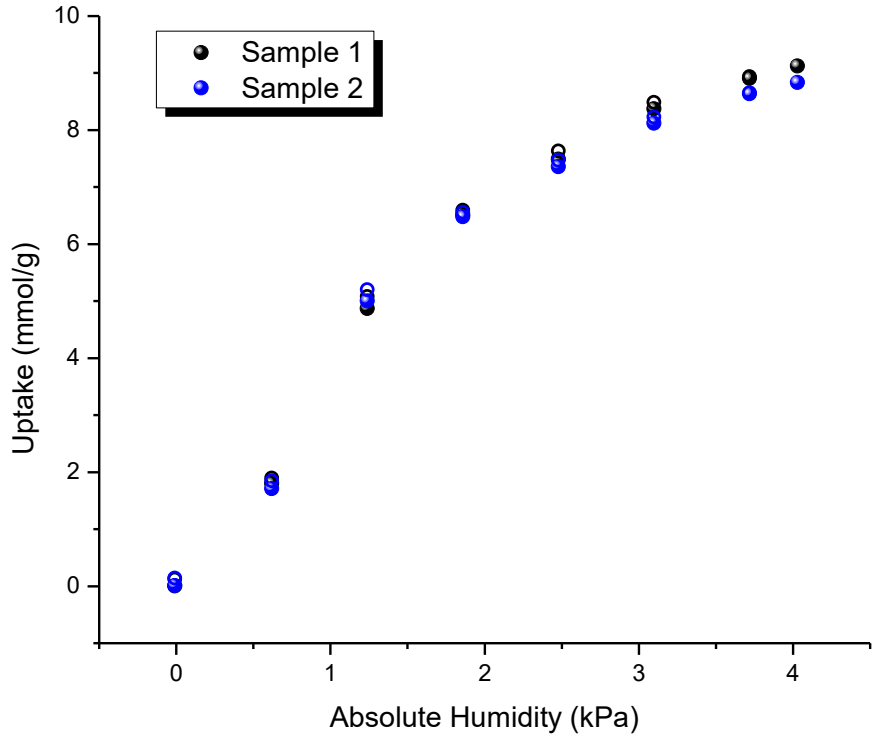

b)

Figure S 15. Comparison of a) CO_2 isotherms and b) H_2O isotherms at 308 K of two different CALF-20 thin film samples, showing excellent reproducibility. Filled circles indicate adsorption points and open circles indicate desorption points.

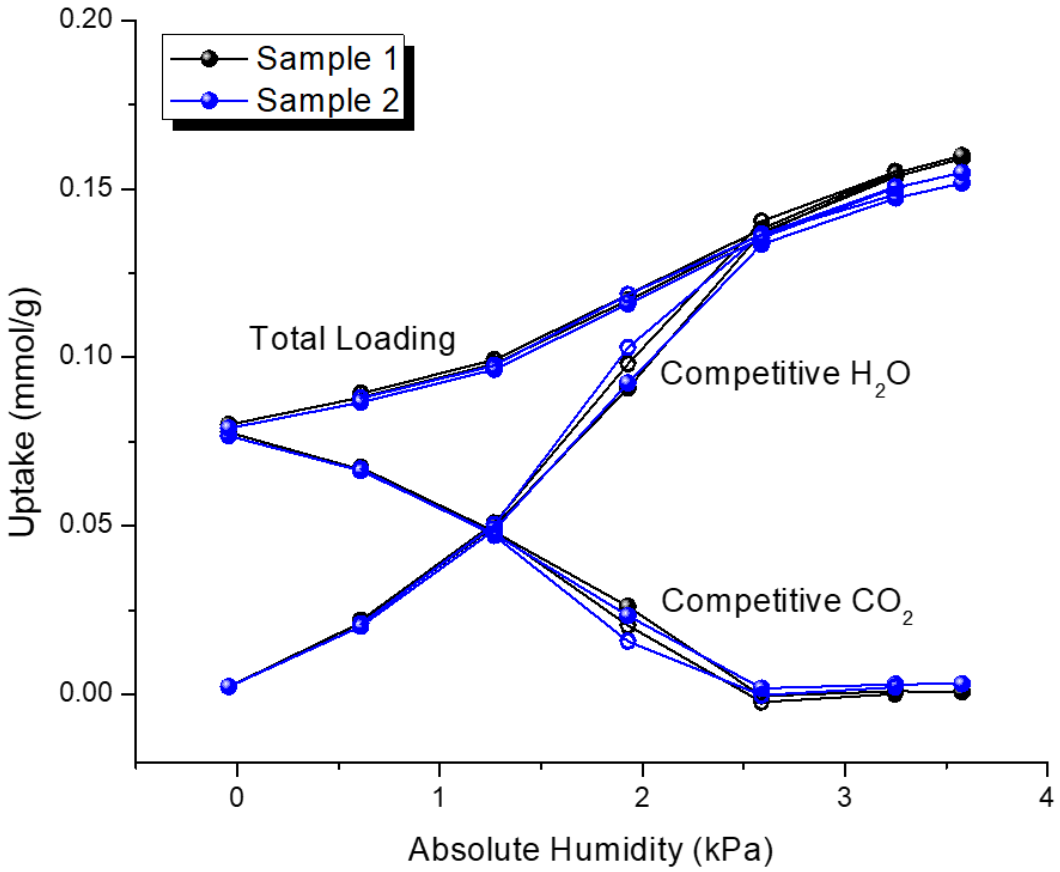

Figure S 16. Comparison of the mixed-gas isotherms at 0.15 bar CO_2 and 308 K of two different CALF-20 thin film samples, showing excellent reproducibility. Filled circles indicate adsorption points and open circles indicate desorption points.

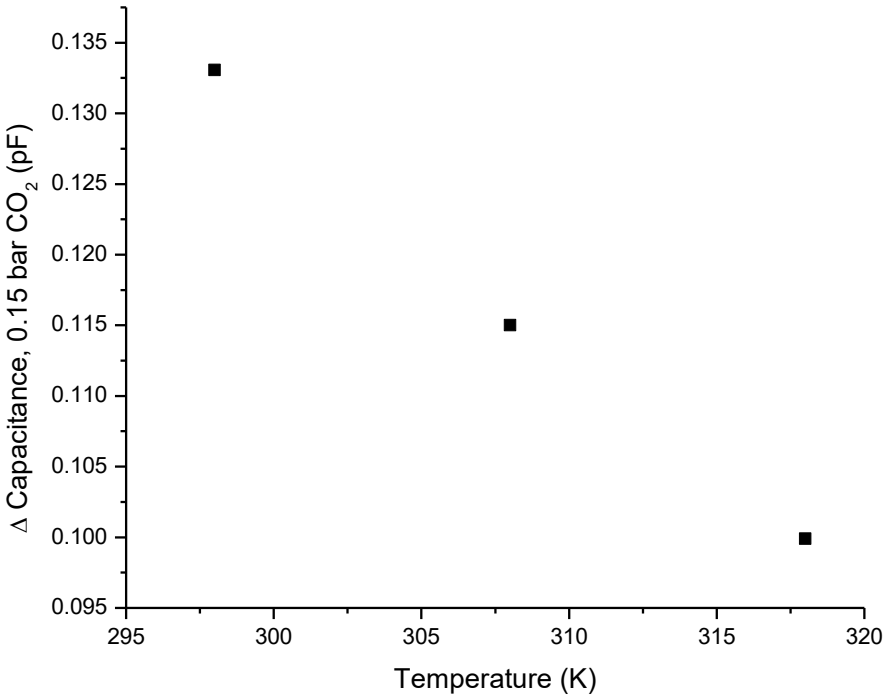

a)

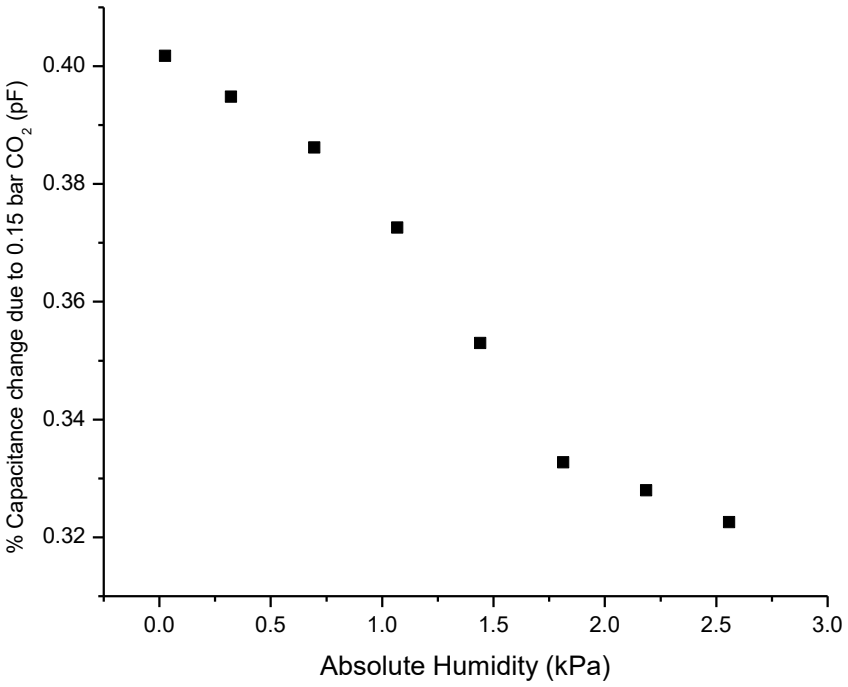

b)

Figure S 17. a) The capacitance change of the IDE due to the introduction of 0.15 bar of CO_2 decreases with increasing temperature. If this is assumed constant over the mixed-gas RH isotherm, we would anticipate the capacitance is over-estimated by the percentages at the given absolute humidities for b) the 298 K mixed-gas adsorption isotherm at 0.15 bar CO_2.

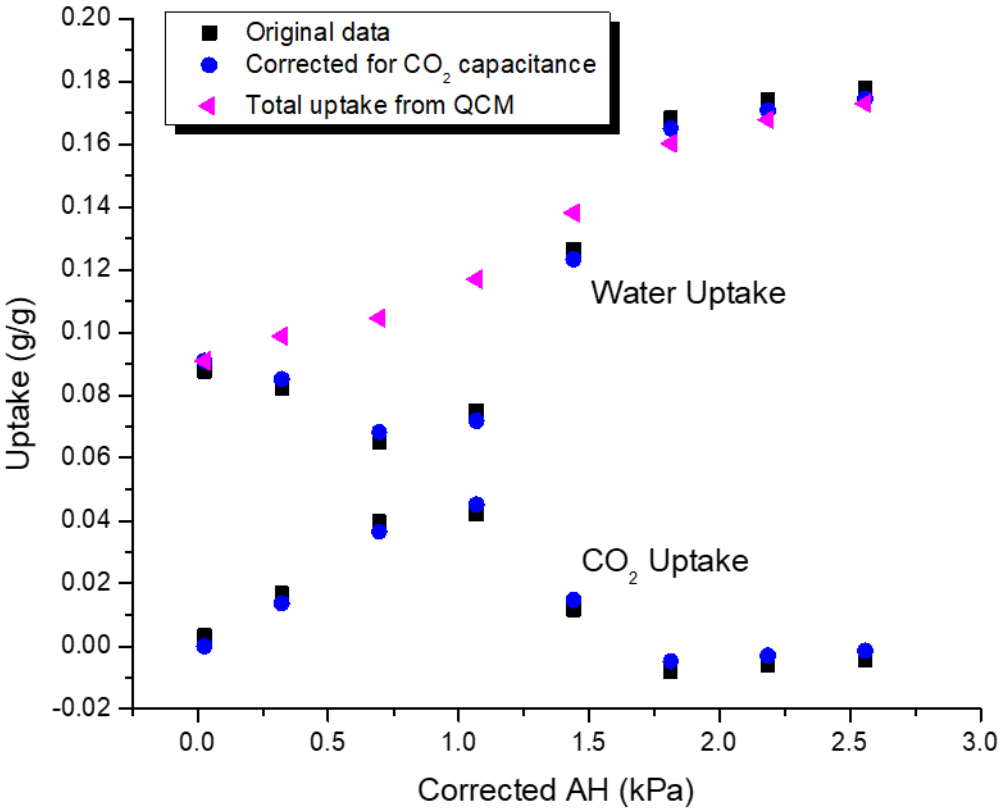

Figure S 18. The mixed-gas RH isotherm at 298 K, 0.15 bar CO_2 is shown above. The total loading as assessed by the QCM is plotted against the IDE-derived water and CO_2 uptake data (black symbols). When a correction is applied to subtract the capacitance of the CO_2 (blue symbols), the change in mixed-gas uptake is very small.

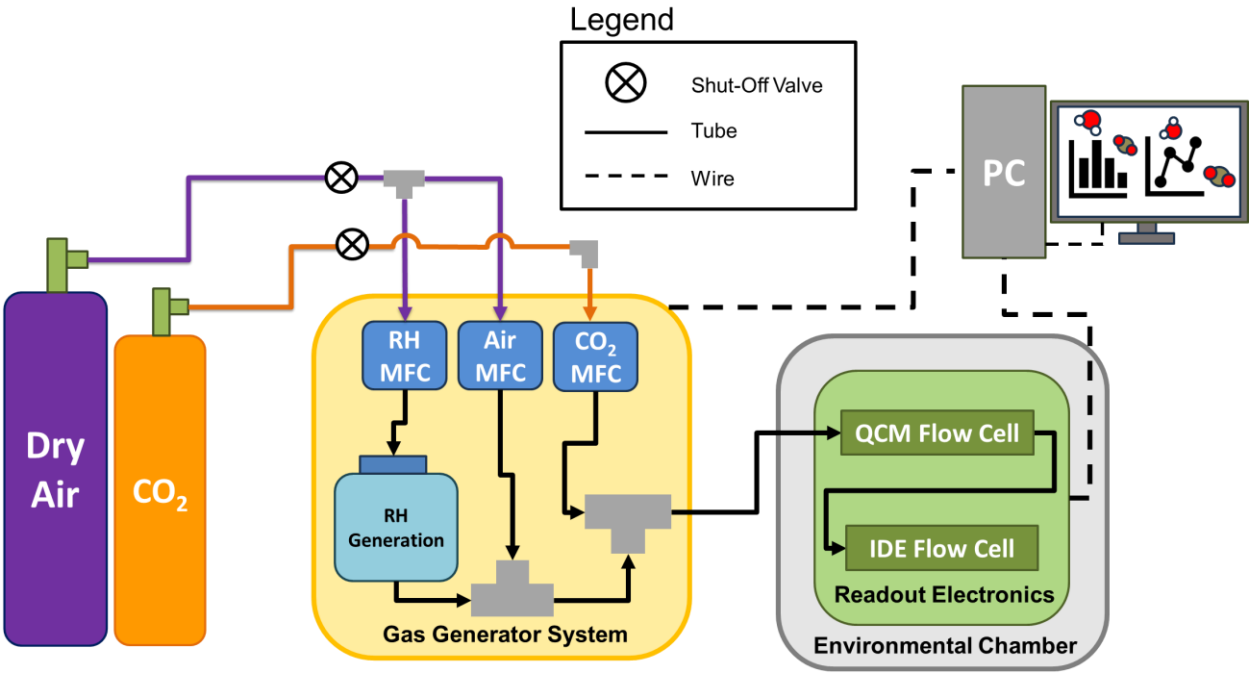

Figure S 19. Schematic of the instrument depicting the gas generator system (gas tanks and yellow box) and sample chamber with flow cells and readout electronics (green box and PC).

3 Additional Discussion

3.1 Discussion of frequency shift conversion to loading

The frequency shift of the composite ($dF_{composite}$) was also assessed to establish the mass of thin film deposited. Under our controlled conditions, the oscillatory frequency of a QCM is inversely proportional to its thickness. The presence of a thin film on the surface of a QCM will thus decrease its frequency. This change, or "shift", can then be applied to calculate a mass measurement using the Sauerbrey equation. The frequency shift is calculated by

$$dF_{composite} = f_{composite} - f_{bare} \quad (2)$$

where f_{bare} is the frequency of the bare QCM before deposition and $f_{composite}$ is the frequency of the composite-coated QCM after the thin film has been activated and is reading a steady dry baseline at the target test temperature.

The change in frequency, or frequency shift, is directly proportional to the mass changes on the surface assuming the Sauerbrey equation holds. This allows us to convert and calculate the loading of a single gas from the center frequency data obtained from the QCM.

The frequency shift of the composite at dry conditions must first be calculated by:

$$dF_{film,dry} = f_{film,dry} - f_{bare} \quad (3)$$

At each gas condition, the frequency shift is calculated by:

$$dF_{film,gas\ condition.} = f_{film,gas\ condition} - f_{film,dry} \quad (4)$$

The ratio of the $dF_{film,\ gas\ condition}$ to $dF_{film,\ dry}$ gives the total loading (g/g) of the film, including the binder.

$$Total\ Uptake\ (g/g) = \frac{dF_{film,gascondition}}{dF_{film,dry}} \quad (5)$$

To calculate the gas uptake of a target material, the total loading is converted to mmol/g using the molecular weight of the introduced gas and is corrected for the mass ratio of the target material in the ink.

3.2 TGA analysis of composite contents

We observed a 7% weight decrease between 30°C to 100°C, which corresponds to water loss from the powder. The temperature was then held at 100°C for two hours to generate a stable baseline for material loading calculations (Figure S 6).

Calculation of material loading using TGA:[3,4]

$$R_{composite} = R_{MOF}(x) + R_{binder}(1 - x) \quad (6)$$

Where:

R_a = residue

x = wt. fraction of MOF loading

Depending on when the degradation residue data is collected, the wt% MOF can change significantly (~10%). Our expected MOF loading based on the mass fractions of starting components (~48%) falls between the two values obtained using different regions of the TGA degradation profile. Given this uncertainty, we have chosen not to recalculate the MOF loading using the TGA-obtained values.

3.3 Discussion of CO_2 capacitance as measured by the IDE

The CO_2 capacitance response is < 2% of the range of the RH response, which we treat as negligible for the purposes of data workup. The CO_2 capacitance response at 0.15 bar (the CO_2 condition of the mixed-gas isotherms reported in this paper) is highest at lower temperatures, and reaches 0.13 pF at 298 K (Figure S 17a). If we assume that this response is constant across the relative humidities of the mixed-gas isotherm at 0.15 bar CO_2, over-estimation of capacitance from CO_2 is < 0.4% for the representative 298 K data set (Figure S 17b). When this flat correction is applied to the 298 K data set, the very small magnitude of this effect is negligible (Figure S 18).

3.4 Discussion of CO_2 and water isotherm differences between thin films and starting powder by several techniques

There are a few possible explanations for the varying CO_2 and water loading of our thin film measurement and powder measurements. The disagreement of various established static and dynamic sorption measurements especially merits further discussion.

Powder measurements by TGA, DVS, and 3Flex

Static sorption measurements collected on the Micromeritics 3Flex give higher water and CO_2 sorption values than the various dynamic sorption methods utilized, including TGA, DVS, and our thin film QCM measurement. Although other publications have shown good agreement between static and

dynamic sorption measurements,[1] it is also well-known that there are several key differences between these techniques that could cause us to observe uptake differences:

1) Activation techniques differ across these measurements. Vacuum activation is achievable with the Micromeritics 3Flex, while dynamic dry air flow is utilized for the other techniques.
2) The presence of a carrier gas in the dynamic techniques. Although CALF-20 is not known to take up large amounts of nitrogen or air, it is possible that small amounts of these components are being adsorbed and competing with CO_2 and water for adsorption sites.
3) Accuracy and precision of controls within these instruments. Although all instruments were recalibrated prior to these measurements, the difference between the error sources, level of control, and expected accuracy of the volumetric technique employed by the 3Flex and the gravimetric techniques employed by the other methods may be noticeable.
4) Assessing and reaching equilibrium in these measurements. Although every effort was taken to ensure that the powder and thin film measurements were allowed to reach equilibrium at each measurement point, it is possible that equilibrium was not fully reached on the lower-uptake TGA measurements. Our TGA is susceptible to temperature variation due to room temperature; this can cause small variations in uptake and, subsequently, difficulty assessing the "true" equilibrium uptake value in TGA.

Thin film measurements

Previous work by Cohen et al[5] and others[6] shows that certain polymers will partially or fully infiltrate MOF pores and block sorption access. We do not expect the polymer we are using to be able to intercalate into the pores of this MOF to a significant extent. The polymer is omniphobic and sterically bulky, and CALF-20 pore apertures are quite small, lowering the chances of significantly blocked pores. In future work, we hope to study possible polymer infiltration in this material using solid-state NMR measurements, as utilized by previous researchers.[5,6] Since our thin film measurements generally fall in the same range as the established powder techniques, we believe we are obtaining useful and representative data from our thin films.

3.5 Discussion of over-estimation of water loading by IDE seen in 298 K mixed-gas uptake data

The first possible contributor to this over-estimation of the water content by the IDE is that the IDE responds very slightly to the presence of CO_2, as seen in Figure 2b. While this does not impact our single-gas isotherms, which are measured using the QCM, the mixed-gas isotherm water isotherm values may report slightly higher capacitances due to this, causing the water loading from the IDE to appear higher than the water loading from the QCM. If this is the case, we would expect small amounts of error to arise from it, similar to the magnitude seen in Figure S 18. A second possible contributor is the fact that although we are depositing the same material in the same way on both the QCM and the IDE, they are different sensors. The QCM has a planar gold deposition surface, while the IDE consists of patterned gold lines on glass with a ~200 nm step height, 5 micron line width, and 10 micron pitch. It is possible that interactions between water and the IDE surface exist that are not present in the QCM, because of this. If this is the case, we would expect this effect to be only present at high relative humidities, where water might be condensing or collecting differently on those surfaces, and only on the IDE, causing an apparent "over-estimation" of water loading from the IDE compared to the QCM. From our data, it appears that this "over-estimation" of water is more obvious at lower temperatures. We would expect both potential effects to be heightened at lower temperatures: Water condensation should occur more readily at lower temperatures, and according to our data, the CO_2 contribution to capacitance is slightly higher at lower temperatures (Figure S 17a). Further study is underway to narrow down the cause of this small over-estimation.

4 The IAST/RAST Models for Mixture Adsorption

We provide a brief outline of the Ideal Adsorbed Solution Theory (IAST) and Real Adsorbed Solution Theory (RAST) for calculation of mixture adsorption equilibrium. The reader is referred to our related publication[7] for more detailed discussions.

4.1 Gibbsian thermodynamics of mixture adsorption

The Gibbs adsorption equation[8] in differential form is

$$Ad\pi = \sum_{i=1}^{n} q_i d\mu_i \tag{S1}$$

The quantity A is the surface area per kg of framework, with units of m^2 per kg of the framework of the crystalline material; q_i is the molar loading of component i in the adsorbed phase with units moles per kg of framework; μ_i is the molar chemical potential of component i. The spreading pressure π has the same units as surface tension, i.e. N m^{-1}.

The chemical potential of any component in the adsorbed phase, μ_i, equals that in the bulk fluid phase. If the partial fugacities in the bulk fluid phase are f_i, we have

$$d\mu_i = RTd\ln f_i \tag{S2}$$

where R is the gas constant (= 8.314 J mol^{-1} K^{-1}).

Briefly, the basic equation of Ideal Adsorbed Solution Theory (IAST) theory of Myers and Prausnitz[9] is the analogue of Raoult's law for vapor-liquid equilibrium, i.e.

$$f_i = P_i^0 x_i; \quad i = 1, 2, ...n \tag{S3}$$

where x_i is the mole fraction in the adsorbed phase

$$x_i = \frac{q_i}{q_1 + q_2 + ...q_n} \tag{S4}$$

and P_i^0 is the pressure for sorption of every component i, which yields the same spreading pressure, π for each of the pure components, as that for the mixture:

$$\frac{\pi A}{RT} = \int_0^{P_1^0} \frac{q_1^0(f)}{f} df = \int_0^{P_2^0} \frac{q_2^0(f)}{f} df = \int_0^{P_3^0} \frac{q_3^0(f)}{f} df = \ldots \tag{S5}$$

where $q_i^0(f)$ is the *pure* component adsorption isotherm. The units of $\Phi \equiv \frac{\pi A}{RT}$, also called the surface potential,[10–14] are mol kg^{-1}.

The unary isotherm may be described by say the 1-site Langmuir isotherm

$$q^0(f) = q_{sat} \frac{bf}{1+bf}; \quad \theta = \frac{bf}{1+bf} \tag{S6}$$

where we define the fractional *occupancy* of the adsorbate molecules, $\theta = q^0(f)/q_{sat}$. The superscript 0 is used to emphasize that $q^0(f)$ relates the *pure component* loading to the bulk fluid fugacity. For unary isotherms described by the dual-Langmuir-Freundlich model

$$q^0(f) = q_{A,sat} \frac{b_A f^{\nu A}}{1+b_A f^{\nu A}} + q_{B,sat} \frac{b_B f^{\nu B}}{1+b_B f^{\nu B}} \tag{S7}$$

each of the integrals in eq (S5) can be evaluated analytically. The integration yields for component *i*,

$$\begin{aligned} \Phi \equiv \frac{\pi A}{RT} &= \int_{f=0}^{P_i^0} \frac{q_i^0(f)}{f} df = \frac{q_{A,sat}}{\nu_A} \ln\left(1+b_A\left(P_i^0\right)^{\nu_A}\right) + \frac{q_{B,sat}}{\nu_B} \ln\left(1+b_B\left(P_i^0\right)^{\nu_B}\right); \\ \Phi \equiv \frac{\pi A}{RT} &= \int_{f=0}^{P_i^0} \frac{q_i^0(f)}{f} df = \frac{q_{A,sat}}{\nu_A} \ln\left(1+b_A\left(\frac{f_i}{x_i}\right)^{\nu_A}\right) + \frac{q_{B,sat}}{\nu_B} \ln\left(1+b_B\left(\frac{f_i}{x_i}\right)^{\nu_B}\right) \end{aligned} \tag{S8}$$

The right hand side of eq (S8) is a function of P_i^0. For multicomponent mixture adsorption, each of the equalities on the right hand side of Eq (S5) must be satisfied. These constraints may be solved using a suitable equation solver, to yield the set of values of , P_2^0, P_3^0 ,.. P_n^0, each of which satisfy eq (S5). The corresponding values of the integrals using these as upper limits of integration must yield the same value of Φ for each component; this ensures that the obtained solution is the correct one.

In the IAST, the adsorbed phase mole fractions x_i are then determined from

$$x_i = \frac{f_i}{P_i^0}; \quad i = 1, 2, \ldots n \tag{S9}$$

The applicability of eqs (S3) and (S9) mandates that all of the adsorption sites within the microporous material are equally accessible to each of the guest molecules, implying a homogeneous distribution of guest adsorbates within the pore landscape, with no preferential locations of any guest species. The circumstances in which this mandate is not fulfilled are highlighted in recent works.[12,13,15,16]

A further key assumption of the IAST is that the adsorption enthalpies and surface areas of the adsorbed molecules do not change upon mixing.[17] If the total mixture loading is q_t, the area covered by the adsorbed mixture is $\frac{A}{q_t}$ with units of m^2 (mol mixture)$^{-1}$. Therefore, the assumption of no surface area change due to mixture adsorption translates as $\frac{A}{q_t} = \frac{Ax_1}{q_1^0\left(P_1^0\right)} + \frac{Ax_2}{q_2^0\left(P_2^0\right)} + \cdots \frac{Ax_n}{q_n^0\left(P_n^0\right)}$; the total mixture loading is q_t is calculated from

$$q_t = q_1 + q_2 ... + q_n = \frac{1}{\frac{x_1}{q_1^0(P_1^0)} + \frac{x_2}{q_2^0(P_2^0)} + ... + \frac{x_n}{q_n^0(P_n^0)}} \tag{S10}$$

in which $q_1^0(P_1^0)$, $q_2^0(P_2^0)$,… $q_n^0(P_n^0)$ are determined from the unary isotherm fits, using the sorption pressures for each component P_1^0, P_2^0, P_3^0,.. P_n^0 that are available from the solutions to equations Eqs (S5), and (S8).

The occurrence of molecular clustering and hydrogen bonding should be expected to applicability of eq (S10) because the surface area occupied by a molecular cluster is different from that of each of the un-clustered guest molecules in the adsorbed phase; see published literature for details.[14,16,18]

The entire set of eqs (S3) to (S10) need to be solved numerically to obtain the loadings, q_i of the individual components in the mixture.

In a number of publications on CO_2 capture from mixtures containing N_2, CH_4, C_2H_4, C_2H_6, C_3H_8, and H_2O using cation-exchanged zeolites,[12,13,15,17,19–24] the IAST has been shown to fail due to non-compliance with one or more of the afore-mentioned tenets.

4.2 Modelling of thermodynamic non-idealities

To quantify non-ideality effects in mixture adsorption, we introduce activity coefficients γ_i into eq (S3) as[7,9,16,17]

$$f_i = P_i^0 x_i \gamma_i \tag{S11}$$

Following the approaches of Myers, Talu, and Siperstein[10,11,25] we model the excess Gibbs free energy for binary mixture adsorption as follows

$$\frac{G^{excess}}{RT} = x_1 \ln(\gamma_1) + x_2 \ln(\gamma_2) \tag{S12}$$

For calculation of the total mixture loading $q_t = q_1 + q_2$ we need to replace eq (S10) by

$$\frac{1}{q_t} = \frac{x_1}{q_1^0(P_1^0)} + \frac{x_2}{q_2^0(P_2^0)} + \left(\frac{1}{q_t}\right)^{excess} \tag{S13}$$

The excess reciprocal loading for the mixture can be related to the partial derivative of the Gibbs free energy with respect to the surface potential at constant composition

$$\left(\frac{1}{q_t}\right)^{excess} = \left.\frac{\partial\left(\frac{G^{excess}}{RT}\right)}{\partial\Phi}\right|_{T,x} \tag{S14}$$

The Margules model for activity coefficients in binary liquid mixtures needs to be modified to include the influence of the surface potential on the activity coefficients

$$\begin{aligned}\ln(\gamma_1) &= x_2^2\left(A_{12} + 2\left(A_{21} - A_{12}\right)x_1\right)\left(1-\exp\left(-C\Phi\right)\right)\\ \ln(\gamma_2) &= x_1^2\left(A_{21} + 2\left(A_{12} - A_{21}\right)x_2\right)\left(1-\exp\left(-C\Phi\right)\right)\end{aligned} \tag{S15}$$

In eq (S15) C is a constant with the units kg mol^{-1}. The introduction of $\left(1-\exp\left(-C\Phi\right)\right)$ imparts the correct limiting behaviors $\Phi \to 0;\ \gamma_i \to 1$ for the activity coefficients in the Henry regime, $f_t \to 0;\ \Phi \to 0$, as the pore occupancy tends to vanishingly small values. As pore saturation conditions are approached, this correction factor tends to unity $\left(1-\exp\left(-C\Phi\right)\right) \to 1$. The Margules coefficients

A_{12}, A_{21} may assume either positive or negative values. The choice of $A_{12} = A_{21} = 0$ in eq (S15), yields unity values for the activity coefficients. We note, in passing, that this correction factor $\left(1-\exp\left(-C\Phi\right)\right)$ is often ignored in the RAST implementations in some published works.[26–29]

For calculation of the total mixture loading $q_t = q_1 + q_2$ we need to replace eq (S10) by

$$\frac{1}{q_t} = \frac{x_1}{q_1^0(P_1^0)} + \frac{x_2}{q_2^0(P_2^0)} + x_1 x_2 \left[A_{12}x_2 + A_{21}x_1\right] C \exp\left(-C\Phi\right) \tag{S16}$$

5 Analysis of Experimental Data on CO_2/H_2O adsorption in CALF-20

Experiments were carried out to determine the component loadings for CO_2/H_2O mixture adsorption in CALF-20 (CALF = Calgary Framework) at three different temperatures 298 K, 308 K, and 318 K In order to test the applicability of the IAST, the data on unary isotherms were first fitted.

5.1 Fitting of unary CO_2 and H_2O isotherms determined at MSI

The unary isotherms for CO_2, and H_2O, measured at three different temperatures 298 K, 308 K, and 318 K in CALF-20 (CALF = Calgary Framework), were fitted with good accuracy using the 1-site Langmuir-Freundlich model:

$$q = \frac{q_{sat} b p^{\nu}}{1 + b p^{\nu}} \tag{S17}$$

In eq (S17), the Langmuir-Freundlich parameter b is temperature dependent

$$b = b_0 \exp\left(\frac{E}{RT}\right) \tag{S18}$$

In eq (S18), E is the energy parameter.

The unary isotherm fit parameters are provided in Table S1.

Figure S 20a,b compare the unary isotherm experiments with the Langmuir-Freundlich parameter fits.

5.2 Isosteric heat of adsorption

The isosteric heat of adsorption, Q_{st}, is defined as

$$Q_{st} = -RT^2 \left(\frac{\partial \ln p}{\partial T}\right)_q \tag{S19}$$

where, the derivative in the right member of eq (S19) is determined at constant adsorbate loading, q. the derivative was determined by analytic differentiation of the combination of eqs (S17), (S18), and eq (S19).

Figure S 20c presents the Q_{st} calculations as function of the molar loadings of the guest species.

5.3 CO_2/H_2O mixture adsorption data vs IAST

The experimental data on the component loadings for $CO_2(1)/H_2O(2)$ mixture adsorption with varying % relative humidity at three different temperatures 298 K, 308 K, and 318 K are indicated by symbols in Figure S 21a,b,c. Here, $\%\text{Relative Humidity} = \frac{p_2}{p_2^{sat}} \times 100$ where p_2 is the partial pressure of water in the bulk gas phase, and p_2^{sat} is the saturation vapor pressure of water. In these experiments, the partial pressures of $CO_2(1)$ was maintained constant at $p_1 = 15$ kPa . The dashed lines are the IAST estimations; for this purpose the unary isotherm fits used are those provided in Table S1. The IAST is in poor agreement with the experimental data; the deviations are higher at lower temperatures, as is to be expected.

5.4 RAST modelling of CO_2/H_2O adsorption in CALF-20

The experimental data on the component loadings of the $CO_2(1)$, and $H_2O(2)$ with varying % relative humidity at three different temperatures 298 K, 308 K, and 318 K measured in this work are indicated by symbols in Figure S 22a,b,c. At each temperature the IAST is unable to quantitatively match the measurements. A close examination also reveals that the deviations from the IAST from the experiments tend to be lowered with increasing temperatures. This is to be expected because of the lowered values of the loadings in the adsorbed phase. The RAST model with fitted Margules parameters, as specified in Table S1, provide a very good match with the measurements, as should be expected.

5.5 List of Tables for Analysis of Experimental Data on CO2/H2O adsorption in CALF-20

Table S1. 1-site Langmuir-Freundlich fits for CO_2 and H_2O determined from fitting unary isotherms measured at three different temperatures 298 K, 308 K, and 318 K in CALF-20.

	$\frac{q_{sat}}{\text{mol/kg}}$	$\frac{b_0}{\text{Pa}^{-1}}$	$\frac{E}{\text{kJ mol}^{-1}}$	ν
CO_2	3	3.597E-10	32	1
H_2O	10.4	1.063E-20	83.2	1.85

Fitted Margules non-ideality parameters for binary CO_2/H_2O mixture adsorption at 298 K, 308 K, and 318 K in CALF-20.

	C / kg mol^{-1}	A_{12}	A_{21}
298 K	0.0591	4.498	-1.478
308 K	0.0591	4.114	-0.646
318 K	0.0591	3.050	2.969

5.6 List of Figures for Analysis of Experimental Data on CO2/H2O adsorption in CALF-20

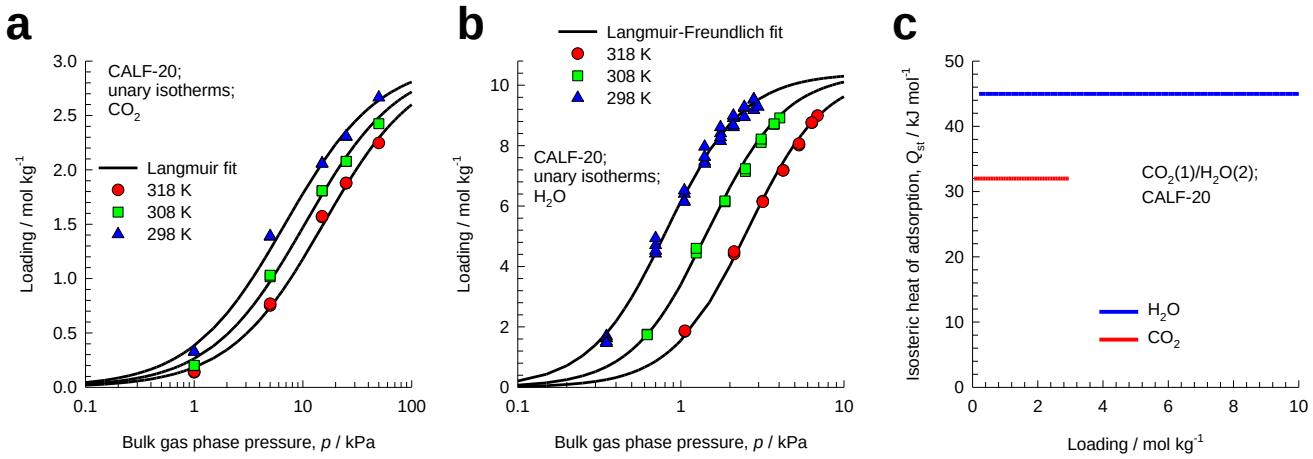

Figure S 20. (a, b) Unary isotherms for (a) CO_2, and (b) H_2O, measured at three different temperatures 298 K, 308 K, and 318 K in CALF-20. The continuous solids are 1-site Langmuir-Freundlich model fits using the parameters specified in in Table S1. (c) Isosteric heats of adsorption for CO_2, and H_2O, plotted as a function of the molar loadings; the Qst calculations are based on eqs (S17), (S18), and eq (S19).

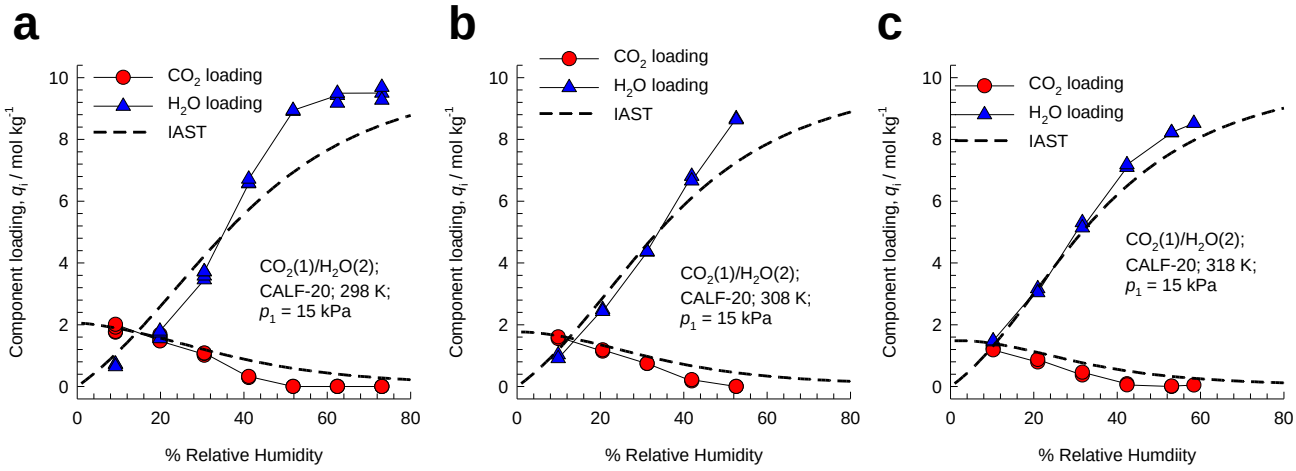

Figure S 21. (a, b, c) Experimental data on the component loadings for $CO_2(1)/H_2O(2)$ mixture adsorption with varying % relative humidity at three different temperature 298 K, 308 K, and 318 K measured in this work are indicated by symbols. In these experiments, the partial pressures of $CO_2(1)$ was maintained constant at $p_1 = 15$ kPa .The dashed lines are the IAST estimations; for this purpose the unary isotherm fits used are those provided in Table S1.

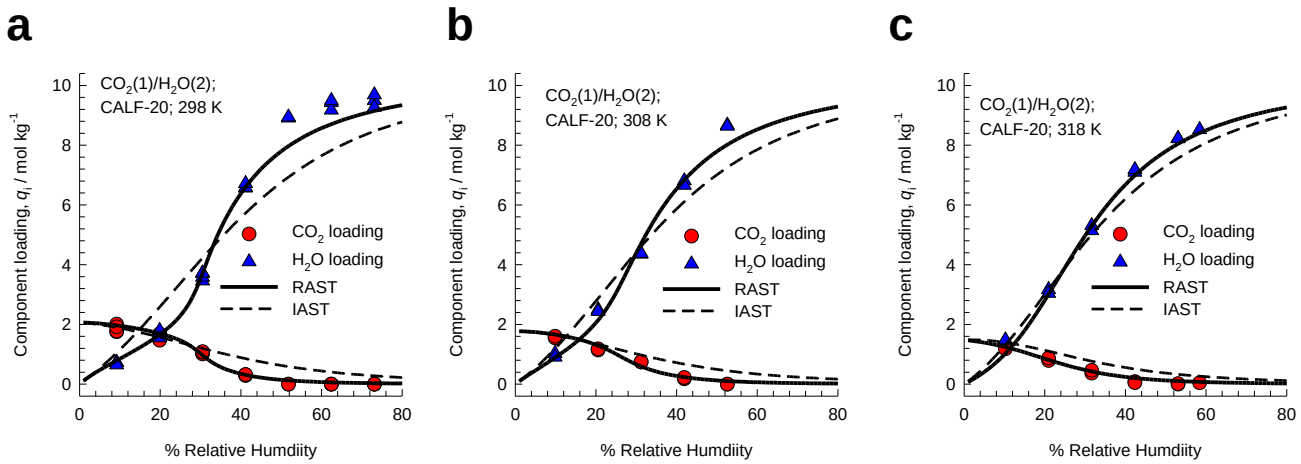

Figure S 22. Experimental data obtained in this work (indicated by symbols) on component loadings for $CO_2(1)/H_2O(2)$ mixture adsorption in CALF-20 at (a) 298 K, (b) 308 K, and (c) 318 K. The total pressure in the bulk gas phase is 15 kPa with varying % relative humidity. The dashed lines are the IAST estimations; for this purpose, the unary isotherm fits are provided in Table S1, The continuous solid lines are the estimations using RAST calculations using fitted Margules parameters provided in Table S1.

6 Nomenclature

Latin alphabet

A	surface area per kg of framework, m^2 kg^{-1}
b_i	Langmuir-Freundlich parameter, $Pa^{-\nu}$
C	constant used in eq (S15), kg mol^{-1}
E	energy parameter, J mol^{-1}
n	number of species in the mixture, dimensionless
p_i	partial pressure of species i in mixture, Pa
p_t	total system pressure, Pa
p_2^{sat}	saturation vapor pressure of water, Pa
P_i^0	sorption pressure, Pa
q_i	component molar loading of species i, mol kg^{-1}
$q_{i,sat}$	molar loading of species i at saturation, mol kg^{-1}
q_t	total molar loading in mixture, mol kg^{-1}
R	gas constant, 8.314 J mol^{-1} K^{-1}
%RH	% relative humidity, dimensionless
T	absolute temperature, K
x_i	mole fraction of species i in adsorbed phase, dimensionless
y_i	mole fraction of species i in the bulk fluid phase, dimensionless

Greek alphabet

γ_i	activity coefficient of component i in adsorbed phase, dimensionless

μ_i	molar chemical potential, J mol^{-1}
ν	Freundlich exponent, dimensionless
π	spreading pressure, N m^{-1}
ρ	framework density, kg m^{-3}
Φ	surface potential, mol kg^{-1}

Subscripts

i	referring to component *i*
t	referring to total mixture
sat	referring to saturation conditions

7 References

(1) Lin, J.-B.; Nguyen, T. T. T.; Vaidhyanathan, R.; Burner, J.; Taylor, J. M.; Durekova, H.; Akhtar, F.; Mah, R. K.; Ghaffari-Nik, O.; Marx, S.; Fylstra, N.; Iremonger, S. S.; Dawson, K. W.; Sarkar, P.; Hovington, P.; Rajendran, A.; Woo, T. K.; Shimizu, G. K. H. A Scalable Metal-Organic Framework as a Durable Physisorbent for Carbon Dioxide Capture. *Science* **2021**, *374* (6574), 1464–1469. https://doi.org/10.1126/science.abi7281.

(2) Chen, Z.; Ho, C.-H.; Wang, X.; Vornholt, S. M.; Rayder, T. M.; Islamoglu, T.; Farha, O. K.; Paesani, F.; Chapman, K. W. Humidity-Responsive Polymorphism in CALF-20: A Resilient MOF Physisorbent for CO_2 Capture. *ACS Mater. Lett.* **2023**, *5* (11), 2942–2947. https://doi.org/10.1021/acsmaterialslett.3c00930.

(3) Satheeshkumar, C.; Yu, H. J.; Park, H.; Kim, M.; Lee, J. S.; Seo, M. Thiol–Ene Photopolymerization of Vinyl-Functionalized Metal–Organic Frameworks towards Mixed-Matrix Membranes. *J. Mater. Chem. A* **2018**, *6* (44), 21961–21968. https://doi.org/10.1039/C8TA03803A.

(4) Mondal, P.; Cohen, S. M. Self-Healing Mixed Matrix Membranes Containing Metal–Organic Frameworks. *Chem. Sci.* **2022**, *13* (41), 12127–12135. https://doi.org/10.1039/d2sc04345a.

(5) Duan, P.; Moreton, J. C.; Tavares, S. R.; Semino, R.; Maurin, G.; Cohen, S. M.; Schmidt-Rohr, K. Polymer Infiltration into Metal–Organic Frameworks in Mixed-Matrix Membranes Detected in Situ by NMR. *J. Am. Chem. Soc.* **2019**, *141* (18), 7589–7595. https://doi.org/10.1021/jacs.9b02789.

(6) Baumann, A. E.; Beaucage, P. A.; Vallery, R.; Gidley, D.; Nieuwendaal, R. C.; Snyder, C. R.; Ilavsky, J.; Chen, F.; Stafford, C. M.; Soles, C. L. Assessing Composite Structure in Metal–Organic Framework-Polymer Mixed-Matrix Membranes. *Chem. Mater.* **2024**, *36* (6), 3022–3033. https://doi.org/10.1021/acs.chemmater.4c00283.

(7) Krishna, R.; van Baten, J. M. Elucidating the Failure of the Ideal Adsorbed Solution Theory for CO2/H2O Mixture Adsorption in CALF-20. *Sep. Purif. Technol.* **2025**, *352*, 128269. https://doi.org/10.1016/j.seppur.2024.128269.

(8) Ruthven, D. M. *Principles of Adsorption and Adsorption Processes*; John Wiley & Sons, 1984.

(9) Myers, A. L.; Prausnitz, J. M. Thermodynamics of Mixed-Gas Adsorption. *AIChE J.* **1965**, *11* (1), 121–127. https://doi.org/10.1002/aic.690110125.

(10) Talu, O.; Myers, A. L. Rigorous Thermodynamic Treatment of Gas Adsorption. *AIChE J.* **1988**, *34* (11), 1887–1893. https://doi.org/10.1002/aic.690341114.

(11) Siperstein, F. R.; Myers, A. L. Mixed-Gas Adsorption. *AIChE J.* **2001**, *47* (5), 1141–1159. https://doi.org/10.1002/aic.690470520.

(12) Krishna, R.; van Baten, J. M. Elucidation of Selectivity Reversals for Binary Mixture Adsorption in Microporous Adsorbents. *ACS Omega* **2020**, *5* (15), 9031–9040. https://doi.org/10.1021/acsomega.0c01051.

(13) Krishna, R.; van Baten, J. M. Using Molecular Simulations for Elucidation of Thermodynamic Nonidealities in Adsorption of CO2-Containing Mixtures in NaX Zeolite. *ACS Omega* **2020**, *5* (32), 20535–20542. https://doi.org/10.1021/acsomega.0c02730.

(14) Krishna, R.; Van Baten, J. M. Water/Alcohol Mixture Adsorption in Hydrophobic Materials: Enhanced Water Ingress Caused by Hydrogen Bonding. *ACS Omega* **2020**, *5* (43), 28393–28402. https://doi.org/10.1021/acsomega.0c04491.

(15) Krishna, R.; van Baten, J. M. Investigating the Non-Idealities in Adsorption of CO2-Bearing Mixtures in Cation-Exchanged Zeolites. *Sep. Purif. Technol.* **2018**, *206*, 208–217. https://doi.org/10.1016/j.seppur.2018.06.009.

(16) Krishna, R.; van Baten, J. M. Fundamental Insights into the Variety of Factors That Influence Water/Alcohol Membrane Permeation Selectivity. *J. Membr. Sci.* **2024**, *698*, 122635. https://doi.org/10.1016/j.memsci.2024.122635.
(17) Krishna, R.; Van Baten, J. M. How Reliable Is the Ideal Adsorbed Solution Theory for the Estimation of Mixture Separation Selectivities in Microporous Crystalline Adsorbents? *ACS Omega* **2021**, *6* (23), 15499–15513. https://doi.org/10.1021/acsomega.1c02136.
(18) Krishna, R.; van Baten, J. M. Hydrogen Bonding Effects in Adsorption of Water−Alcohol Mixtures in Zeolites and the Consequences for the Characteristics of the Maxwell−Stefan Diffusivities. *Langmuir* **2010**, *26* (13), 10854–10867. https://doi.org/10.1021/la100737c.
(19) Krishna, R.; van Baten, J. M.; Baur, R. Highlighting the Origins and Consequences of Thermodynamic Non-Idealities in Mixture Separations Using Zeolites and Metal-Organic Frameworks. *Microporous Mesoporous Mater.* **2018**, *267*, 274–292. https://doi.org/10.1016/j.micromeso.2018.03.013.
(20) Wilkins, N. S.; Rajendran, A. Measurement of Competitive CO2 and N2 Adsorption on Zeolite 13X for Post-Combustion CO2 Capture. *Adsorption* **2019**, *25* (2), 115–133. https://doi.org/10.1007/s10450-018-00004-2.
(21) Hefti, M.; Marx, D.; Joss, L.; Mazzotti, M. Adsorption Equilibrium of Binary Mixtures of Carbon Dioxide and Nitrogen on Zeolites ZSM-5 and 13X. *Microporous Mesoporous Mater.* **2015**, *215*, 215–228. https://doi.org/10.1016/j.micromeso.2015.05.044.
(22) van Zandvoort, I.; Ras, E.-J.; Graaf, R. de; Krishna, R. Using Transient Breakthrough Experiments for Screening of Adsorbents for Separation of C2H4/CO2 Mixtures. *Sep. Purif. Technol.* **2020**, *241*, 116706. https://doi.org/10.1016/j.seppur.2020.116706.
(23) van Zandvoort, I.; van der Waal, J. K.; Ras, E.-J.; de Graaf, R.; Krishna, R. Highlighting Non-Idealities in C2H4/CO2 Mixture Adsorption in 5A Zeolite. *Sep. Purif. Technol.* **2019**, *227*, 115730. https://doi.org/10.1016/j.seppur.2019.115730.
(24) Wang, Y.; LeVan, M. D. Adsorption Equilibrium of Binary Mixtures of Carbon Dioxide and Water Vapor on Zeolites 5A and 13X. *J. Chem. Eng. Data* **2010**, *55* (9), 3189–3195. https://doi.org/10.1021/je100053g.
(25) Talu, O.; Zwiebel, I. Multicomponent Adsorption Equilibria of Nonideal Mixtures. *AIChE J.* **1986**, *32* (8), 1263–1276. https://doi.org/10.1002/aic.690320805.
(26) Sochard, S.; Fernandes, N.; Reneaume, J.-M. Modeling of Adsorption Isotherm of a Binary Mixture with Real Adsorbed Solution Theory and Nonrandom Two-Liquid Model. *AIChE J.* **2010**, *56* (12), 3109–3119. https://doi.org/10.1002/aic.12220.
(27) Mittal, N.; Bai, P.; Siepmann, J. I.; Daoutidis, P.; Tsapatsis, M. Bioethanol Enrichment Using Zeolite Membranes: Molecular Modeling, Conceptual Process Design and Techno-Economic Analysis. *J. Membr. Sci.* **2017**, *540*, 464–476. https://doi.org/10.1016/j.memsci.2017.06.075.
(28) Calleja, G.; Jimenez, A.; Pau, J.; Domínguez, L.; Pérez, P. Multicomponent Adsorption Equilibrium of Ethylene, Propane, Propylene and CO2 on 13X Zeolite. *Gas Sep. Purif.* **1994**, *8* (4), 247–256. https://doi.org/10.1016/0950-4214(94)80005-7.
(29) Kaur, H.; Marshall, B. Real Adsorbed Solution Theory Model for the Adsorption of CO2 from Humid Gas on CALF-20. ChemRxiv November 16, 2023. https://doi.org/10.26434/chemrxiv-2023-2cp2c.